United States
Department of
Agriculture

Forest Service

Forest
Products
Laboratory

Research
Note

FPL–RN–0283

JMFA—A Graphically Interactive Java Program That Fits Microfibril Angle X-ray Diffraction Data

Steve P. Verrill
David E. Kretschmann
Victoria L. Herian

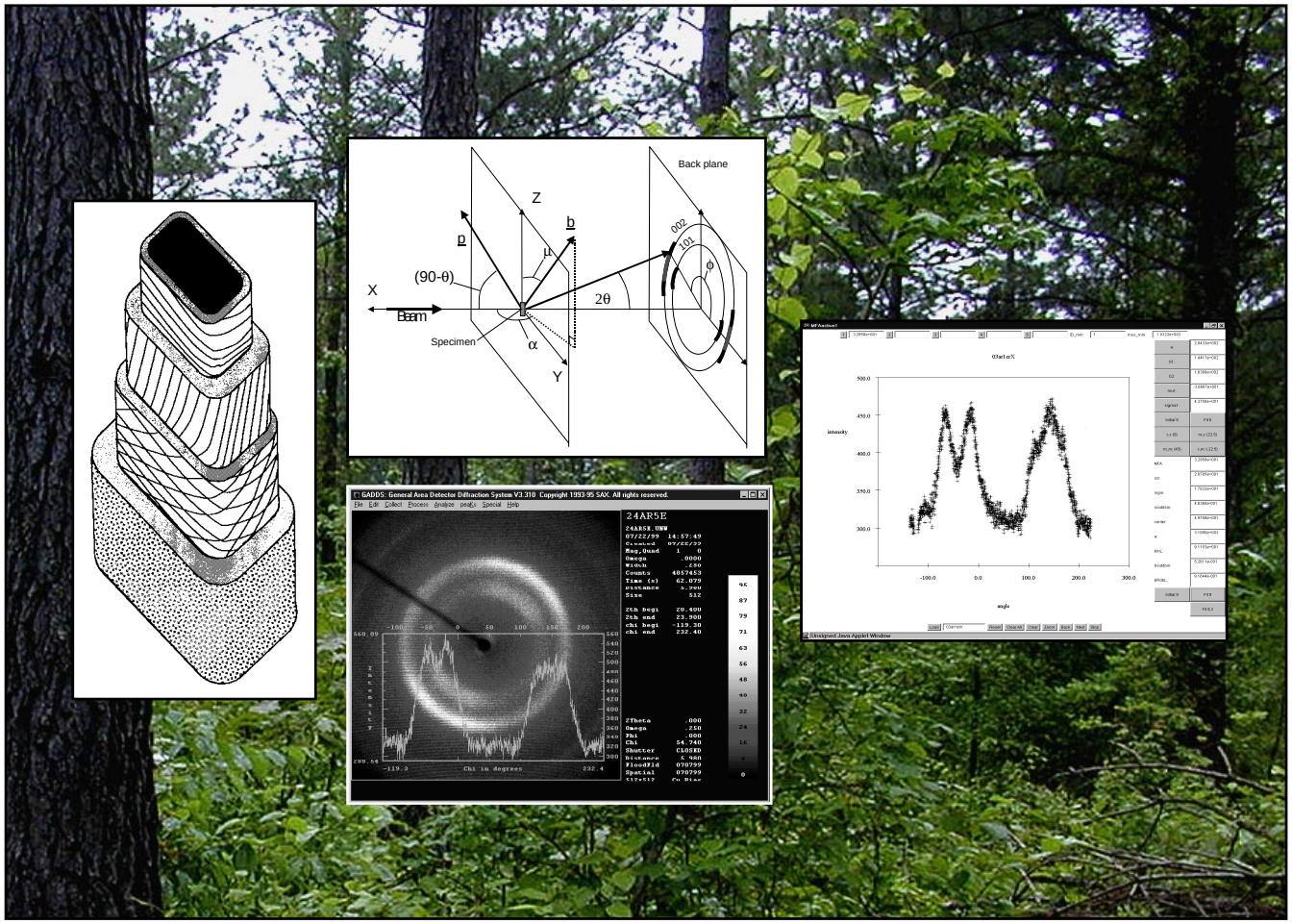

Abstract

Because much of our future timber resource is expected to come from short rotation plantations, we need to develop silvicultural practices that will improve the quality of the timber coming from these plantations. Short rotation plantations tend to produce timber with a higher percentage of juvenile wood, which has substantially lower mechanical property values than does mature wood. Measuring the microfibril angle (MFA) of wood gives important clues about the characteristics of the wood and can be used as a silvicultural tool to improve the quality of a plantation. In this report, we discuss a graphically interactive Java computer program that permits a user to estimate MFA from X-ray diffraction profiles. Given an MFA and a wood cell rotation pair (μ, α), this program makes use of Cave's theory to predict the locations of the eight high intensity X-ray spots on the back plane. Nonlinear least squares techniques are then used to find the (μ, α) pair that yields a broadened form of the eight spots that best fits the empirical X-ray diffraction data. The program can be run as an applet over the World Wide Web, or it can be downloaded and run as an application on a user's own machine. Because this program is based on a more complete physics model than earlier programs, we expect that it will yield more accurate MFA estimates. Preliminary comparisons of the new program's MFA estimates with microscopy based estimates are encouraging. A complete evaluation of the accuracy of the program's estimates will appear in a subsequent paper.

Keywords: microfibril angle, X-ray diffraction, Java, interactive graphics, mechanical properties of wood, forest monitoring

November 2001

Verrill, Steve P.; Kretschmann, David E.; Herian, Victoria L. 2001. JMFA—A graphically interactive Java program that fits microfibril angle X-ray diffraction data. Res. Note FPL-RN-0283. Madison, WI: U.S. Department of Agriculture, Forest Service, Forest Products Laboratory. 44 p.

A limited number of free copies of this publication are available to the public from the Forest Products Laboratory, One Gifford Pinchot Drive, Madison, WI 53705–2398. This publication is also available online at www.fpl.fs.fed.us. Laboratory publications are sent to hundreds of libraries in the United States and elsewhere.

The Forest Products Laboratory is maintained in cooperation with the University of Wisconsin.

Contents

JMFA — A Graphically Interactive Java Program That Fits Microfibril Angle X-ray Diffraction Data

Steve P. Verrill, Mathematical Statistician
David E. Kretschmann, Research General Engineer
Victoria L. Herian, Statistician
Forest Products Laboratory, Madison, Wisconsin

1 Introduction

X-ray diffraction techniques have the potential to decrease the time required to determine microfibril angles dramatically. This decrease will permit us to gain a better understanding of the relationships between microfibril angle (MFA) and the mechanical properties of wood, which will in turn permit us to do a better job of managing the changing wood resource. In this paper, we discuss a new curve fitting tool that permits us to reduce the time required to evaluate MFA X-ray diffraction patterns. Further, because this tool reflects the underlying physics more accurately than existing tools, we expect it to yield more accurate estimates of MFA.

1.1 Background

Much of our future timber supply is expected to come from improved softwood and hardwood trees grown on managed plantations or from small-diameter timber removed during forest management operations. This short age-rotation resource will contain higher proportions of juvenile wood than the present resource.

Boone and Chudnoff (1972) raised early concerns about the quality of plantation grown material. Their research was conducted on 8-year-old plantation Caribbean pine (*Pinus caribaea* Morelet) from Puerto Rico. In their study of small clear specimens, specific gravity, bending stiffness, and strength values were reduced by more than 50% from the published values for virgin timber of the same species. At about the same time, research conducted at North Carolina State University on clear wood of loblolly pine demonstrated that the problem was juvenile wood, not plantation wood (Pearson and Gilmore 1971). This research demonstrated that juvenile wood has substantially lower mechanical property values than mature wood, which generally accounts for the inferior properties of short rotation plantation wood compared with those of long rotation timber.

One can respond to these reductions in properties by attempting to improve silvicultural practices. Improved silvicultural practices require improved tools for monitoring stand quality. Microfibril angle measurements hold promise as one such tool.

1.2 Importance of Microfibril Angle

Wood cells are made up of multiple layers: a primary layer, P, and three secondary layers, S1, S2, and S3 (Figure 1). The secondary layers consist of helically arranged cellulose microfibrils oriented toward the long axis of the tracheid. The thickest of the secondary layers is the S2 layer, and its properties strongly influence the properties of the wood fiber. Microfibril angle is measured as the angular deviation from the vertical cell wall of the microfibrils in the S2 layer.

The orientations of the microfibrils in the S2 layer of juvenile wood tracheids vary widely both within and among trees of a species. In loblolly pine (*Pinus taeda* L.), for example, the MFA in mature wood is small, averaging about 5 to 10 degrees. In juvenile loblolly, the MFA is large; it averages 25 to 35 degrees, is often as high as 50 degrees in the annual rings next to the pith, and decreases outward in the juvenile core (Megraw 1986, Bendtsen and Senft 1986). The decrease in MFA often continues well beyond the juvenile core. For example, Ying and others (1994) found that MFAs in tracheids of fast-grown loblolly pines decreased from 33 degrees at age 1 to 23 degrees at age 10 and 17 degrees at age 22. Bendtsen and Senft (1986) reported that MFAs had not yet attained stable values in 30-year-old loblolly pines.

There is a strong belief that the MFA of the S2 layer of the woody cell wall is a critical factor in the mechanical behavior of wood (Megraw 1986). Orientation of the S2 MFA has a significant influence on the tensile strength, stiffness, and shrinkage of wood.

Data from Bendtsen and Senft (1986), based on a 30-year-old loblolly pine plantation, suggest that the differences in strength properties between juvenile and mature wood cannot be accounted for solely by differences in specific gravity. Their data also suggest that the volume of earlywood and the high MFAs of the earlywood tracheids in the early juvenile wood growth rings might be far more important. Cave and Walker (1994) concluded that MFA plays a major role in the pronounced decrease in stiffness (modulus of elasticity) for juvenile wood in fast-grown radiata pine and that MFA is a factor that can be used as a selection tool in plantation management.

A strong relationship exists between MFA and longitudinal shrinkage. In tests on juvenile wood of radiata pine (*Pinus radiata* D. Don), Harris and Meylan (1965) showed that longitudinal shrinkage increased sharply while tangential shrinkage decreased at MFAs greater than 25 degrees. Longitudinal shrinkage was low at MFAs below 25 degrees, while tangential shrinkage increased as MFAs fell below 15 degrees. Ying and others (1994) showed that MFAs of 25 degrees or greater corresponded to the outer boundary of the 10-year juvenile core in loblolly pine.

Modeling suggests that the relative thickness of the P, S1, and S3 layers contributes significantly to the variability of longitudinal shrinkage (Cave 1976).

Given that our future timber supply is expected to come from shorter rotation forests, definitive information is needed on the influence of MFA on lumber properties so that selection and utilization methods can be adjusted accordingly.

1.3 Methods of Measuring MFA

The traditional methods for determining the MFA of the S2 layer have been based on the orientation of the cross-field pit apertures (Dadswell and Nicholls 1959, 1960; Donaldson 1991), the enhancement of checks or the maximum extinction position using polarizing light (Echols 1955, Foracs 1961), the use of fluorescence light microscopy to enhance checks (Marts 1955), and the orientation of iodine crystals that form in induced checks (Senft and Bendtsen 1985). Much of the current literature has been developed using these techniques, but these methods are slow and tedious.

X-ray diffraction techniques have also been used to determine MFA (Cave 1966, Harris and Meylan 1965, Meylan 1967). Recently, Evans and others (1996), Cave and Robinson (1998), Kretschmann and others (1998), and Lichtenegger and others (1998) have done work to refine X-ray diffraction as a much more rapid technique for measuring MFA. This technique uses the diffraction pattern created by the interaction of X-rays with wood tissue to determine MFA (Figure 2). A group of fibers is irradiated perpendicular to the fiber length by a narrow, monochromatic X-ray beam. A diffraction pattern is produced by the crystalline cellulose structure and recorded on film or by an electronic detector. This pattern consists of a series of arcs that are spaced apart

by a number of well-defined concentric circles. See the back plane of Figure 2. The diameters of the concentric circles are indications of the spacing of the crystalline planes within the cellulose crystalline fibrils.

In this paper, we discuss a new graphically interactive Java program (see, for example, `http://java.sun.com/java2/whatis/`) that yields rapid analyses of microfibril X-ray diffraction patterns. In addition to leading to speedy analyses, this program makes use of an improved model of the underlying physics that should yield more accurate MFA estimates.

2 The Program

2.1 Heuristic Justification of Our Approach

Cave (1966) derived an equation that relates the locations of the spots of high X-ray intensity on the back plane of the X-ray apparatus to the Bragg angle associated with the X-rays, the rotation of the wood cell, and the MFA. This equation applies to cells with square cross sections. In the Appendix we provide a derivation of this equation. (The derivation does not appear in Cave's paper.) We also develop a method for finding analytic solutions to the equation. Figure 2 provides an illustration of the relevant geometry. The equation is

$$\tan(\theta)\cos(\alpha) + \sin(\alpha)\cos(\phi) + \cot(\mu)\sin(\phi) = 0 \tag{1}$$

where θ is the Bragg angle (11.35 degrees for X-rays of wavelength 1.54 angstroms), μ is the MFA, α is 90 degrees plus the rotation of the "front" face of the wood cell beyond perpendicular to the incoming beam, and ϕ is the azimuthal angle of the spot on the "2θ circle" on the back plane (measured counterclockwise from the East). $\alpha = 90$ degrees if the front face is perpendicular to the incoming beam (Figure 3).

The equation yields two spots for each face of the cell. We claim that distinct μ, α pairs lead to distinct collections of eight spots. Thus given the locations of the eight spots, we know the MFA μ (as well as the cell rotation $\alpha - 90$).

We do not attempt to prove this claim mathematically in this paper. (In a future paper, "X-ray diffraction bright spots as predictors of a unique MFA, cell rotation pair," we will present a mathematical treatment of this claim.) However, Figures 4 through 16 permit the reader to view a visual "proof." In these figures, the upper left circle corresponds to the spots on the back plane for a 10 degree MFA. (The angular location, ϕ, of a spot is calculated by solving Equation (1).) The upper right circle corresponds to a 20 degree MFA. The center left circle corresponds to a 30 degree MFA, the center right to a 40 degree MFA, the bottom left to a 50 degree MFA, and the bottom right to a 60 degree MFA. The different figures correspond to different wood cell rotations (0, 10, 20, 22.5, 30, 40, 45, 50, 60, 67.5, 70, 80, and 90 degrees). (A rotation of size r where $45\,\text{deg} \leq r \leq 90\,\text{deg}$ yields the same pattern as a rotation of size $90 - r$ except that the locations are reflected across a north-south axis, and the positions of front (back) face spots are exchanged with the positions of right (left) spots.)

The open squares indicate the locations on the back plane of reflections from the face that was the front face (closest to the beam source and perpendicular to the beam) before rotation. The black squares indicate the locations on the back plane of reflections from the face that was the back face before rotation. The upward pointing arrows indicate the locations on the back plane of the reflections from the face that was the right face before rotation (to the right as one faces the cell from the beam source). The downward pointing arrows indicate the locations on the back plane of reflections from the face that was the left face before rotation.

Several points are clear from the pictures. First, on each left and right half circle the extreme spots get further apart as the MFA increases. Second, for a 0 degree wood cell rotation if we broaden the spots via gaussian noise, the resultant X-ray intensity profiles have central peaks on both the right half and left half back plane circles (Figure 17). (When we plot intensity on the back plane circle versus angle measured in a counterclockwise direction from the east, the right half circle is plotted to the left [smaller angles] and the left half circle is plotted to the right [larger angles].) For a 22.5 degree wood cell rotation, the broadened profiles have a double peak on the right half back plane circle and a central peak on the left half back plane circle (Figure 18). For a 45 degree wood cell rotation, the broadened profiles have double peaks on both half circles (Figure 19). For a 67.5 (or -22.5) degree wood cell rotation, the broadened profiles have a central peak on the right half back plane circle and a double peak on the left half circle (Figure 20). Finally the relative relationships between the front/back spots and the right/left spots change as the rotation changes.

Cave (1966) argued that for the case of a 0 degree rotation (Figure 4), the outer edges of the two main intensity profiles (Figure 17) would be due primarily to a broadening of the four points associated with the front and back faces of the wood cells. For a 0 degree rotation and MFA μ, these spots can be shown (via Equation (1)) to lie at angles $-\mu$, μ, $180-\mu$, and $180+\mu$ (where these angles are measured in a counterclockwise direction and the 0 degree spot direction is to the east in Figure 4). Consider the broadened point at angular location $-\mu$. If it is broadened in a gaussian fashion, and if we can neglect the contributions of the other points to the left edge of the first profile in Figure 17, then the left edge of the first profile in Figure 17 is given by

$$\text{intensity}(\phi) = a + b \times \exp(-(\phi - (-\mu))^2/(2\sigma^2))$$

where ϕ is the angle and σ is the broadening factor. The left point of inflection of this left profile can be shown to lie at $-\mu-\sigma$, and the line that is tangent to the profile at the inflection point can be shown to intersect the background level (intensity $= a$) at angle $-\mu-2\sigma$. Similarly, if we can neglect the contributions of all but one point to the right edge of the left profile in Figure 17, the line that is tangent to the left profile at its right point of inflection intersects the background level at angle $\mu+2\sigma$.

For practical reasons, Meylan (1967) had previously recommended that

$$T = (\text{right intersection point} - \text{left intersection point})/2$$

be used as an indirect measure of MFA. By his argument, Cave established that

$$T \approx (\mu + 2\sigma - (-\mu - 2\sigma))/2 = \mu + 2\sigma. \tag{2}$$

He further argued that there were empirical reasons to believe that

$$\sigma \approx \mu/3. \tag{3}$$

Combining Equations (2) and (3), we obtain

$$\mu \approx 0.6T \tag{4}$$

where T is half the distance between the intercept of the tangent line to the right inflection point of a profile with the background and the intercept of the tangent line to the left inflection point of a profile with the background. For years, some version of Equation (4) has been used to analyze MFA X-ray diffraction profiles. (Evans (1999) develops an alternate approach.) Initially, the tangent lines were drawn by hand. More recently, Stuart and Evans (1994) and Kretschmann and others (1998)

automated the process by assuming that a left (or right) profile (Figures 17 – 20) could be fit by a single Gaussian (rather than by a combination of four Gaussians). Nonlinear least squares techniques were used to perform this fit and then it was possible to calculate the T value from the left and right inflection points of the one fitted Gaussian. (This procedure will tend to yield tangent lines that are too shallow and thus MFA values that are too large.)

Cave's 1966 procedure will be appropriate if the following asumptions hold

1. the intensity spots associated with the front and back faces are located at angles $-\mu$, μ, $180 - \mu$, and $180 + \mu$,

2. the left and right edges of a profile are only affected by a single one of the four spots associated with the profile, and

3. we can approximate the point broadening σ with a function of μ (such as $\sigma \approx \mu/3$).

As can be seen in Figures 4 – 16, as the front face is rotated away from a position perpendicular to the incoming beam, assumption 2 becomes invalid. For example, in Figure 7 one can see that for a rotation of 22.5 degrees, the left edge of the left profile in Figure 18 (due to the right half of the circle in Figure 7) will be a combination of both the front face and left face spot broadenings. The right edge of the left profile in Figure 18 will be a combination of both the right face and back face broadenings.

Also, as the front face is rotated away from a position perpendicular to the incoming beam, assumption 1 becomes invalid. For example, from Equation (1) we can calculate that for the right half circle on the back plane, the location of the front face spot in the 30 MFA degree circle in Figure 8 (30 degree rotation) is -23.59 degrees. The location of the back face spot is 23.59 degrees.

In our program we avoid Cave's 1966 assumptions by taking advantage of the relationship between the eight point profiles and the μ, α pair to estimate μ on the basis of the profiles. In particular, we perform a nine parameter nonlinear least squares in which we find a linear combination of *all* eight Gaussians that best fits the observed X-ray intensity profile. Such an approach would not have been feasible in 1966. It has only become feasible with the massive increase in computing power that we have seen in the last 30 years.

The nine parameters of the nonlinear least squares model are as follows:

- μ, the MFA
- α, 90 degrees plus the rotation (counterclockwise looking down at the top of the wood cell) of the front face of the wood cell beyond perpendicular to the X-ray beam (Figure 3)
- *sigin*, the standard deviation (broadening factor) associated with the two least extreme (inner) spots on each half circle
- *soutdsin*, the ratio of the standard deviation associated with the two most extreme (outer) spots on each half circle to the the standard deviation associated with the two least extreme (inner) spots
- *center*, the angular location of the minimum between the two sets of broadened spots. Given the geometry illustrated in Figures 4 – 16, the value of *center* would be 90 degrees (counterclockwise from the east direction on the page). However, a data set might have been generated in such a way that this value is something other than 90 degrees. For example, our apparatus yields a value of approximately 54.7 degrees for this minimum location.
- a, the background X-ray intensity

- *binL*, the intensity associated with the inner spots on the right half circle (the *left* profile on the plot presented to a user of the program, hence the L)
- *boutdbin*, the ratio of the intensity of an outer peak to that of an inner peak
- *bRdbL*, the ratio of the intensity of the left half circle on the back plane to the right half circle (again the ratio of the right to the left profiles on the plot presented to the user of the program, hence the RL)

The a and *center* parameters are artifacts of the data collection process. The b (intensity) and s (broadening) parameters have some physical meaning but they also contain ad hoc elements in our current implementation. We know of no physical reason why the intensity of the left half profile should differ from the intensity of the right half. However, we do see this in data so we provided for it via the *bRdbL* parameter. There are physical arguments that suggest that there might be differences between the front (back) and right (left) faces in intensity and variability. We provide for these differences in an ad hoc fashion via the *boutdbin* and *soutdsin* parameters.

2.2 Predicted Intensity

Let $l_1 < l_2 < \ldots < l_8$ be the locations of the spots obtained from Cave's equation. (See Section 6.3 in the Appendix for the mathematical details. The l's will depend on the value of the μ, α pair.) $l_1, \ldots, l_4$ correspond to the right half circle on the back plane (the left profile in the plot presented to the user of our program) and $l_5, \ldots, l_8$ correspond to the left half circle on the back plane (the right profile in the plot presented to the user of our program).

Define

$$\begin{aligned}
\sigma_{\text{in}} &\equiv sigin \\
\sigma_{\text{out}} &\equiv soutdsin \times sigin \\
a_1(\phi) &\equiv (\phi - l_1)^2/(2\sigma^2_{\text{out}}) \\
a_2(\phi) &\equiv (\phi - l_2)^2/(2\sigma^2_{\text{in}}) \\
a_3(\phi) &\equiv (\phi - l_3)^2/(2\sigma^2_{\text{in}}) \\
a_4(\phi) &\equiv (\phi - l_4)^2/(2\sigma^2_{\text{out}}) \\
a_5(\phi) &\equiv (\phi - l_5)^2/(2\sigma^2_{\text{out}}) \\
a_6(\phi) &\equiv (\phi - l_6)^2/(2\sigma^2_{\text{in}}) \\
a_7(\phi) &\equiv (\phi - l_7)^2/(2\sigma^2_{\text{in}}) \\
a_8(\phi) &\equiv (\phi - l_8)^2/(2\sigma^2_{\text{out}})
\end{aligned}$$

The predicted intensity at angle ϕ that is fit via the nonlinear least squares program to the observed intensity is

$$\begin{aligned}
\text{predicted} = \; & a + binL \times [boutdbin \times \exp(-a_1(\phi)) + \exp(-a_2(\phi)) \\
& + \exp(-a_3(\phi)) + boutdbin \times \exp(-a_4(\phi))] \\
& + bRdbL \times binL \times [boutdbin \times \exp(-a_5(\phi)) + \exp(-a_6(\phi)) \\
& + \exp(-a_7(\phi)) + boutdbin \times \exp(-a_8(\phi))]
\end{aligned} \tag{5}$$

The nonlinear least squares program returns as an estimate of the MFA μ the value that minimizes the sum (over the angles at which intensity was measured) of the squared differences between the observed intensity and the intensity predicted from Equation (5).

Two versions of the program have been developed, an "applet" version and an "application" version. The applet version can be run via a browser over the Web. The application version can be downloaded and run completely on the user's own machine. For network security reasons the two versions must differ slightly. For that reason we discuss them separately here.

2.3 The Applet

2.3.1 Getting data to and from the applet

Currently, the Java applet expects data in the following form: The data file should be an ASCII text file, not a proprietary word processing or spreadsheet document. Text files can be produced by proprietary word processing or spread sheet programs. On personal computers they tend to have extensions such as ".txt" or ".prn".

The text file should begin with a data set's name. The name *cannot contain spaces*. Next, the text file should contain two columns of X-ray diffraction pattern data. The first column should contain angle values (for example, −180 to 180 or 0 to 360), and the second column should contain the corresponding intensity values. The angles in the first column must be increasing but they do not have to be increasing in constant increments. At the end of this angle/intensity data set, a new data set can be placed. Again, it must begin with a line that contains only the data set name. Here is an excerpt from the beginning of the `mfa_demo_input` file that is the default applet data file. A user can run the applet on this data file by going to `http://www1.fpl.fs.fed.us/mfa.html`.

```
03ar1erX
-0.1364E+03          0.3084E+03
-0.1363E+03          0.3084E+03
-0.1362E+03          0.3125E+03
-0.1361E+03          0.3144E+03
-0.1360E+03          0.3144E+03
.
.
.
0.2232E+03          0.3016E+03
0.2233E+03          0.3026E+03
0.2234E+03          0.3084E+03
0.2235E+03          0.3084E+03
0.2236E+03          0.3084E+03
12br1erX
-0.1364E+03          0.3259E+03
-0.1363E+03          0.3259E+03
-0.1362E+03          0.3275E+03
-0.1361E+03          0.3343E+03
-0.1360E+03          0.3343E+03
.
.
.
```

A version of data set 03ar1erX that has been cleaned by the removal of a glitch is plotted in Figure 22. A cleaned version of data set 12br1erX is plotted in Figure 24.

Currently, the applet can handle at most 100 data sets in the data file. Also, each data set

can contain at most 3,700 observations (for a possible total of 370,000 angle/intensity pairs in the data file). If the reader wishes to use this applet and either of these restrictions presents a problem, please contact Steve Verrill at the USDA Forest Service Forest Products Laboratory (`steve@ws13.fpl.fs.fed.us` or 608-231-9375).

We describe below how to obtain a Java application version of this applet that can be run locally on your machine with access to your file system. It can read the data file directly from your file system and write the results files directly to your file system. However, for quite good security reasons, Java applets cannot read from or write to your file system. Thus, if you do not want to download and install the application version of this applet but do want to run it on your data, you must anonymous ftp the data file to `www1.fpl.fs.fed.us` and put it in the pub/data directory. (Anonymous ftp directions can be found at `http://www1.fpl.fs.fed.us/anonftp0.html`.) Then, after you start the applet, replace "mfa_demo_input" in the first applet window with the name of your data file and "mfa_demo_output" in the first applet window with the prefix that you want for your output files. These names *must be unique to you* to avoid intermixing your results with those of another user.

2.3.2 First applet window

When a user goes to `http://www1.fpl.fs.fed.us/mfa.html`, the applet is started and the user is presented with a small window (Figure 21) that contains the data file and results file prefix input boxes mentioned in the previous section. The window also contains a text field in which the user must specify the Bragg angle associated with their experimental setup. In addition, the window contains a text field in which the user specifies the approximate location in degrees of the minimum intensity between the left and right profiles of their data. After the four text fields are filled in, the user clicks the **Go** button and the main applet window pops up. (Figure 22.) This may take a number of seconds if the data set is large.

2.3.3 Main applet window

After the main applet window pops up, a user should maximize it to ensure that all text fields are displayed.

As described in the heuristic justification section, the program performs a nine parameter nonlinear least squares fit to estimate the MFA. To perform such a fit, we need reasonable initial estimates of the parameters. We obtain these by first performing a simpler six parameter nonlinear squares fit. *This fit must be completed before a nine parameter fit is attempted.* The predicted intensity in this case is given by

$$\begin{aligned} \text{predicted}(\phi) &= a + b_1 \times \exp(-(\phi - \mu_1)^2/(2\sigma_1^2)) \\ &\quad + b_2 \times \exp(-(\phi - (\mu_1 + 180))^2/(2\sigma_2^2)) \end{aligned}$$

where the parameters are a, b_1, b_2, μ_1, σ_1, and σ_2. (We have produced some confusing notation here. In the theoretical discussion we have used μ to denote the MFA. Here we are using μ_1 to denote the center of a peak.) In other words, we model the complete profile as a double Gaussian in which the two peaks may have different heights and widths. Initial estimates for this six parameter fit are obtained automatically by clicking on the **Initial 6** button in the right panel (Figure 22). The resulting initial intensity curve appears as a blue line overlaying the data. If this initial curve is even *roughly* reasonable, then a user can obtain a good six parameter fit by clicking on the **Fit 6** button in the right panel. The resulting six parameter fit appears as a green curve overlaying the data. The corresponding fitted a, b_1, b_2, μ_1, and σ_1 values appear in the boxes in the right

panel next to these names, and the resulting initial estimates for the nine parameters in the more complicated model appear next to their names in the right panel.

Occasionally, the initial curve for the six parameter fit is not a reasonable starting point for the nonlinear least squares program. A user quickly learns to identify such situations from the appearance of the blue overlay. In this case the user must provide improved initial estimates. This can be done in two ways. The user can type initial estimates into the text fields next to the **a**, **b1**, **b2**, **mu1**, and **sigma1** buttons or the user can use the mouse to identify good initial values:

- To use the mouse to identify an initial a value, click the **a** button. A horizontal blue line will appear at the height corresponding to the current a value. Now click the mouse on the plot at a height that is approximately even with the plot's baseline. The first horizontal blue line will be replaced with a new one that corresponds to the height selected by the mouse click. This new a value will also appear in the text field next to the **a** button. In addition, the old initial fit overlay will be replaced by a new (cyan) overlay based on the new initial parameter values.

- To use the mouse to identify an initial b_1 value, click the **b1** button. A horizontal blue line will appear at the height corresponding to the current $a + b_1$ value. Now click the mouse on the plot at a height that is approximately even with the *leftmost* main peak's maximum. The first horizontal blue line will be replaced with a new one that corresponds to the height selected by the mouse click. The new b_1 value (calculated as click height minus the a value) will also appear in the text field next to the **b1** button. In addition, the old initial fit overlay will be replaced by a new (cyan) overlay based on the new initial parameter values.

- To use the mouse to identify an initial b_2 value, click the **b2** button. A horizontal blue line will appear at the height corresponding to the current $a + b_2$ value. Now click the mouse on the plot at a height that is approximately even with the *rightmost* main peak's maximum. The first horizontal blue line will be replaced with a new one that corresponds to the height selected by the mouse click. The new b_2 value (calculated as click height minus the a value) will also appear in the text field next to the **b2** button. In addition, the old initial fit overlay will be replaced by a new (cyan) overlay based on the new initial parameter values.

- To use the mouse to identify an initial μ_1 value, click the **mu1** button. A vertical blue line will appear at the ϕ value corresponding to the current μ_1 value. Now click the mouse on the plot at a ϕ value that is approximately at the midpoint of the *leftmost* main peak. The first vertical blue line will be replaced with a new one that corresponds to the ϕ value selected by the mouse click. The new μ_1 value will also appear in the text field next to the **mu1** button. In addition, the old initial fit overlay will be replaced by a new (cyan) overlay based on the new initial parameter values.

- To use the mouse to identify an initial σ_1 value (which is used for both σ_1 and σ_2), click the **sigma1** button. A vertical blue line will appear at the ϕ value corresponding to the current μ_1 value. A second vertical blue line will appear at the ϕ value corresponding to $\mu_1 + \sigma_1$. Now click the mouse on the plot at a ϕ value that is approximately equal to an improved $\mu_1 + \sigma_1$ estimate. (Ideally, this should be at a point at which the curve is at about 60% of its maximum height. However, the initial σ_1 value does not have to be very close at all to the correct value for the subsequent nonlinear least squares to succeed.) The second vertical blue line will be replaced with a new one that corresponds to the ϕ value selected by the mouse click. The new σ_1 value (calculated as the click ϕ value minus μ_1) will also appear in the text

field next to the **sigma1** button. In addition, the old initial fit overlay will be replaced by a new (cyan) overlay based on the new initial parameter values.

After a user is satisfied with a new initial fit overlay (one set of button clicks should be sufficient), they can proceed with a fit of the two single peaks model by clicking the **Fit 6** button. The result of a nonlinear least squares fit of this model will appear as a green overlay (replacing the blue or cyan initial conditions overlay).

The initial estimates for the nine parameter fit are obtained as follows:

- $\boldsymbol{\mu}$ The initial estimate of the MFA is $0.8 \times 0.6 \times (\sigma_1 + \sigma_2)$. This is $0.8 \times 0.6 \times T$ where the T value is that of Stuart and Evans (1994). The 0.6 multiplier appears in Cave (1966). The 0.8 value is an ad hoc multiplier that we have found leads to initial MFA estimates that are more in accord with microscopy based estimates.
- **rot** The initial wood cell rotation estimate is 0 degrees. However, see the descriptions of the **c,c**; **nc,c**; **c,nc**; and **nc,nc** buttons given later in this section.
- **sigin** The initial estimate of the *sigin* value is $\mu/3$ which is in accord with a suggestion made by Cave (1966).
- **soutdsin** The initial estimate of the *soutdsin* value is 1.0.
- **center** The initial estimate for *center* is provided by the user in the start-up window. The estimate should be in degrees and should be typed into the text field next to the "Minimum location" label.
- **a** The initial a value is the estimated a from the six parameter fit.
- **binL** The initial $binL$ value is $b_1/2$ where b_1 is the estimated b_1 from the six parameter fit.
- **boutdbin** The initial *boutdbin* value is 1.0.
- **bRdbL** The initial $bRdbL$ value is b_2/b_1.

Any of these "automatic" initial estimates can be altered by typing in the box next to the relevant name. The curve based on these initial estimates can be viewed by clicking on the **Initial 9** button in the right panel. The initial curve then appears as an orange overlay on the data.

Before proceeding with a nine parameter fit, we need to consider the possibility that the initial estimate of the rotation of the wood cells should not be 0 degrees. As noted in the section on the heuristic justification for our approach, if the front faces of the wood cells in a specimen are not perpendicular to the X-ray beam, then the location of the eight bright spots will change. As we saw in Figure 17, if the front faces are perpendicular to the beam, the complete broadened profile should contain left and right profiles with central peaks. As we saw in Figure 18, if the front faces of the wood cells are rotated 22.5 degrees in a counterclockwise direction (looking down at the specimen from above) the complete profile should contain a left profile with two noncentral peaks and a right profile with a central peak. If a user sees this pattern, they should click the **nc,c** (this stands for noncentral, central) button on the right panel prior to performing the nine parameter fit. As we saw in Figure 19, if the front faces of the wood cells are rotated 45 degrees in a counterclockwise direction, the complete profile should contain left and right profiles that each contain two noncentral peaks. If a user sees this pattern, they should click the **nc,nc** button on the right panel prior to performing the nine parameter fit. Finally, as we saw in Figure 20, if the front faces of the wood cells are rotated 67.5 degrees in a counterclockwise direction (or -22.5 degrees

in a clockwise direction) the complete profile should contain a left profile with a central peak and a right profile with two noncentral peaks. If a user sees this pattern, they should click the **c,nc** button on the right panel prior to performing the nine parameter fit.

A user performs a nine parameter fit by clicking on either the **Fit 9** button or the **Fit 9,3** button. If the **Fit 9** button is clicked, one nonlinear least squares fit is performed and the resulting predicted intensity values are plotted as a red overlay. The final parameter estimates are displayed in the "MFA," "rot," "sigin," "soutdsin," "center," "a," "binL," "boutdbin," and "bRdbL" text fields. The MFA estimate also appears in the panel at the top of the window. If the fit is the first nine parameter fit of the data set, the MFA estimate appears next to the **1** button. If the fit is the second nine parameter fit of the data set, the MFA estimate appears next to the **2** button. And so on. When more than one fit is performed, the ID of the fit that corresponds to a minimum mean sum of squares is placed in the box to the right of "ID_min" in the top panel. The corresponding minimum sum of squares is placed in the box to the right of "mss_min" in the top panel. Currently, the program permits at most 5 nine parameter fits of a particular data set. (Of course one can always reload the data set to obtain additional fits. However this should not be necessary.) See below for a description of how results are saved to a file.

If the **Fit 9,3** button is clicked, three fits are performed. They differ only in the initial estimate of the rotation. The three fits use -22.5 degrees, 0 degrees, and 22.5 degrees as the initial rotation estimates. Of these three fits, the fit associated with the smallest sum of squares is reported in the appropriate box on the top panel.

2.3.4 Load, Reset, Clear All, Clear, and Zoom buttons

If a user never clicks the **Load** button, the data sets are simply presented in the order in which they appear in the data file. The **Load** button permits a user to load a particular one of the data sets in the data file. The user must type the data set name (as it appears in the data file) into the text field next to the **Load** button and then click the **Load** button. After a file has been loaded via the **Load** button, the files are presented in the order in which they appear in the data file but beginning with the file just loaded.

The **Reset**, **Clear All**, **Clear**, and **Zoom** buttons can be used to remove "glitches" in the data.

- A user *excludes rectangular regions* of data by pushing a mouse button down at one corner of the rectangle, holding the button down while moving the pointer to the opposite corner of the rectangle, and then releasing the button. While a user is performing this movement, an animated red rectangle appears that outlines the current exclusion region. After the button is released the outline of the rectangle turns black, and it can no longer be moved.

- If a user wants to look at only the data that has not been excluded, the user should press the **Zoom** button. A sequence of zooms may be performed.

- Currently, the program does not permit a user to unzoom a single zoom. However, a user can reactivate all of the data by pressing the **Reset** button at the bottom of the page. A user can see all of the inactivated rectangles by performing a fit and then by clicking the appropriate recall button at the top of the page.

- The data in an inactivated rectangle can be reactivated if the rectangle is "cleared." A user clears a rectangle by clicking a mouse button in it (all rectangles that contain this point will be cleared) and then clicking on the **Clear** button at the bottom of the page. All rectangles

that are shown on the current page (in the current "zoom state") will be cleared if the user clicks the **Clear All** button at the bottom of the page.

2.3.5 Buttons 1, 2, 3, 4, and 5 in the top panel

As explained above, a user fits the active data by sequentially clicking the **Initial 6**, **Fit 6**, and **Fit 9** or **Fit 9,3** buttons in the right hand panel.

As we explained above, after a nine parameter fit has been performed, an estimate of the MFA appears in one of the boxes at the top of the page. At any time prior to a click of the **Load**, **Back**, **Next**, or **Stop** buttons, this fit can be recalled by clicking the top panel button (buttons **1** – **5**) associated with the fit.

2.3.6 Writing results to files

The **Back** button loads the preceeding data set in the data file. The **Next** button loads the next data set in the data file. The **Stop** button ends the execution of the program. *If a nine parameter fit has been performed*, then when the next **Load**, **Back**, **Next**, or **Stop** button is clicked, information is written to two results files. To a file titled xxx.ests (where xxx is the output prefix provided by the user in the startup box) in the pub/data anonymous ftp space on www1.fpl.fs.fed.us, the applet writes the ID and the nine parameter estimates (including the MFA estimate) calculated from the *most recently displayed* nine parameter fit. To a file titled xxx.inact (where xxx is the output prefix provided by the user in the startup box), the applet writes the ID, the number of inactivated rectangles associated with the *most recently displayed* fit, and the pairs of x, y values that define them. These files can be retrieved via anonymous ftp from the pub/data directory of www1.fpl.fs.fed.us. (Anonymous ftp directions can be found at `http://www1.fpl.fs.fed.us/anonftp0.html`.)

2.4 The Application

The application differs from the applet in how it is accessed, in how the data set is read and in how the results are written.

The application expects data in the same form expected by the applet and has the same restrictions on data set size. The data can be located in any directory on your machine to which you have access.

You can download the Java application to have a version of the program that resides on your personal machine. The code is available in both compressed tar and zip form.

The source code, class files, and associated documentation and data files for a **UNIX** (The Open Group, San Francisco, California) machine are included in the file `mfa.src.tar.Z`. You can install and run the program on your machine by following these instructions.

1. Go to `www1.fpl.fs.fed.us/mfa.src.tar.html` and click on the `mfa.src.tar.Z` link.

2. Once you click on this link, a box comes up asking where you want to save the file on your computer. Once you give it a path and file name and click OK, it will be written to that directory.

3. After you receive the file as (for example) `mfa.src.tar.Z`, you will have to uncompress the file with the command (for example) `uncompress mfa.src.tar.Z`, and then untar the resulting file with the command (for example) `tar xvf mfa.src.tar`. This should be done in a directory that lies in the CLASSPATH of your machine.

4. To start the application, type `java MFA_application`.

For more information, please read the README.html, copyright, and disclaimer files.

The source code, class files, and associated documentation and data files for a **Windows** (Microsoft Corporation, Redmond, Washington) machine are included in the file `mfa.src.exe`. You can install and run the program on your machine by following these instructions.

1. Go to `www1.fpl.fs.fed.us/mfa.src.zip.html` and clicking on the `mfa.src.exe` link.

2. Once you click on this link, a box comes up asking where you want to save the file on your computer. Save it in a directory such as `c:\mfa`.

3. Next, you need to open a DOS window. Click the START button, go to PROGRAMS, MS-DOS PROMPT.

4. When the DOS window comes up, go to the directory in which `mfa.src.exe` has been saved (for example, `cd c:\mfa`).

5. Then, while in the directory, type **mfa.src.exe** and the archive will unpack itself.

6. You then need to type `install.bat` to create the necessary subdirectories.

7. You can then run the application by typing `java MFA_application`.

Further information on both the applet and the application can be found at `http://www1.fpl.fs.fed.us/mfa0.html`.

After you have started the application on your computer, a start-up window appears (Figure 23). It contains five text input fields and a **Go** button. In the first text field you need to place the name of the data file. If the data file does not lie in the directory in which you are running the Java application, you need to provide the *full* path name to the data file. Alternatively, you can use the associated **Browse** button to find the data file. After you click on the file in the browse window and then click on the open button in the browse window, the correct path to the file will appear in the text field.

A user needs to fill out the "MFA estimates file" text field (either directly or via the associated **Browse** button) to provide a file to which the fitted parameters (including the estimated microfibril angles) will be written.

A user needs to fill out the "Inactive rectangles file" text field (either directly or via the associated **Browse** button) to provide a file to which the application writes data set IDs, numbers of inactivated rectangles, and pairs of x, y values that define them.

The window also contains a text field in which the user must specify the Bragg angle associated with their experimental setup. Finally, the window contains a text field in which the user specifies the approximate location in degrees of the minimum intensity between the left and right profiles of their data.

After the user has filled in the five text fields, they click on the **Go** button to bring up the main window.

The application has one feature not provided by the applet. It includes a **Print** button in the bottom panel of the main window (Figure 24). Provided that one of the user's printers can handle postscript output, this button permits the user to print the current image displayed in the plotting portion of the main window. Alternatively, the postscript image of the plot can be written to a file (to be printed on someone else's postscript-capable printer).

3 Summary

The changing nature of the nation's timber supply requires improved silvicultural practices, which in turn require improved tools for monitoring stand quality. MFA measurements hold promise as stand quality predictors, and X-ray diffraction techniques appear to represent a practical method for quickly estimating MFAs for large numbers of wood cells. In this report, we have discussed a graphically interactive Java computer program that permits a user to obtain measurements of MFA rapidly from X-ray diffraction patterns. Because this program is based on a more complete physics model than earlier programs, we expect that it will yield more accurate MFA estimates. Preliminary comparisons of the new program's MFA estimates with microscopy based estimates are encouraging. A complete evaluation of the accuracy of the program's estimates will appear in a subsequent paper.

The current version of the program can be run as an applet over the World Wide Web, or it can be downloaded and run as an application on a user's own machine. Both the applet and the application can be accessed at `http://www1.fpl.fs.fed.us/mfa0.html`. We are continuing to evaluate and improve this computer program.

4 Acknowledgment

We thank Dr. Ian Cave for valuable discussions in which he shared his insight into new approaches to the analysis of MFA X-ray diffraction data. We stress, however, that any misconceptions or errors that appear in this paper are entirely our own.

5 References

Bendtsen, B.A. and Senft, J. (1986). "Mechanical and anatomical properties in individual growth rings of plantation-grown eastern cottonwood and loblolly pine." *Wood and Fiber Science.* **18**(1). Pages 23-38.

Boone, R.S. and Chudnoff, M. (1972). "Compression wood formation and other characteristics of plantation-grown *Pinus caribaea*." Rio Piedros, Puerto Rico: USDA For. Serv. Res. Pap. ITF-13, Institute of Tropical Forestry.

Cave, I.D. (1966). "X-ray measurement of microfibril angle." *Forest Products Journal.* **16**(10). Pages 37-42.

Cave, I.D. (1976). "Modeling the structure of the softwood cell wall for computation of mechanical properties." *Wood Science and Technology.* **10**. Pages 19-28.

Cave, I.D., and Robinson, W. (1998). "Measuring microfibril angle distribution in the cell wall by means of X-ray diffraction." *Microfibril Angle in Wood.* B.G. Butterfield editor. International Association of Wood Anatomists. University of Canterbury. New Zealand. Pages 94-107.

Cave, I.D. and Walker, J.C.F. (1994). "Stiffness of wood in fast-grown plantation softwoods." *Forest Products Journal.* **44**(5). Pages 43-48.

Dadswell, H.E. and Nicholls, J.W.P. (1959). "Assessment of wood qualities for tree breeding. I. In *Pinus elliottii* var. *elliottii* from Queensland." Queensland, Australia: Div. of For. Prod. Technol. Paper No. 4.

Dadswell, H.E. and Nicholls, J.W.P. (1960). "Some aspects of wood anatomy in relation to pulping quality and to tree breeding." *Appita.* **13**(5). Pages 161-172.

Donaldson, L.A. (1991). "The use of pit apertures as windows to measure microfibril angle in chemical pulp fibres." *Wood and Fiber Science.* **23**. Pages 290-295.

Echols, R.M. (1955). "Linear relation of fibrillar angle to tracheid length, and genetic control of tracheid length in slash pine." *Tropical Woods.* **102**. Pages 11-22.

Evans, R.E. (1999). "A Variance approach to the X-ray diffractometric estimation of microfibril angle in wood." *Appita Journal.* **52**(4). Pages 283-289,294.

Evans, R., Stuart, S.A., and van der Touw, J. (1996). "Microfibril angle scanning of increment cores by X-ray diffractometry." *Proceedings, Appita general conference, May 6-10, 1996, Auckland, New Zealand*, pages 879-882.

Foracs, O. L. (1961). "Structural weaknesses in softwood pulp tracheids." *Tappi.* **44**. Pages 112-119.

Harris, J.M. and Meylan, B.A. (1965). "The influence of microfibril angle on longitudinal and tangential shrinkage in *Pinus radiata*." *Holzforschung.* **19**(5). Pages 144-153.

Kretschmann, D.E., Alden, H.A., and Verrill, S. (1998). "Variations of microfibril angle in loblolly pine: comparison of iodine crystallization and X-ray diffraction techniques." *Microfibril Angle in Wood*, B.G. Butterfield editor. International Association of Wood Anatomists. University of Canterbury. New Zealand. Pages 157-176.

Lichtenegger, H., Reiterer, A., Tschegg, S., and Fratzl, P. (1998). "Determination of spiral angles of elementary fibrils in the wood cell wall: comparison of small angle X-ray scattering and wide angle X-ray diffraction." *Microfibril Angle in Wood.* B.G. Butterfield editor. International Association of Wood Anatomists. University of Canterbury. New Zealand. Pages 157-176.

Marts, R. O. (1955). "Fluorescence microscopy for measuring fibril angles in pine tracheids." *Stain Technology.* **30**(5). Pages 243-248.

Megraw, R.A. (1986). "Wood quality factors in loblolly pine: the influence of tree age, position in the tree, and cultural practice on wood specific gravity, fiber length and fibril angle." TAPPI Press, pages 1-88.

Meylan, B. A. (1967). "Measurement of microfibril angle by X-ray diffraction." *Forest Products Journal.* **17**(5). Pages 51-58.

Pearson, R.G. and Gilmore, R.C. (1971). "Characterization of the strength of juvenile wood of loblolly pine." *Forest Products Journal.* **21**(1). Pages 23-30.

Senft, J.F. and Bendtsen, B.A. (1985). "Measuring micofibrillar angles using light microscopy." *Wood and Fiber Science.* **17**(4). Pages 564-567.

Stuart, S. and Evans R. (1994). "X-ray diffraction estimation of the microfibril angle variation in eucalypt wood." *Appita.* **48**(3). Pages 197-200.

Ying, L., Kretschmann, D.E., and Bendtsen, B.A. (1994). "Longitudinal shrinkage in fast-grown loblolly pine plantation wood." *Forest Products Journal.* **44**(1). Pages 58-62

6 Appendix — Cave's Equation

Cave (1966) derived an equation for the locations of the spots of high X-ray intensity on the back plane of the X-ray apparatus. This equation applies to cells with square cross sections. Because versions of this derivation that we have seen have been sketchy or opaque (there was no derivation in Cave's 1966 paper), we provide our own derivation here. We also convert Cave's equation into a quadratic equation that we solve analytically.

6.1 Derivation of Cave's Equation

The equation is

$$\tan(\theta)\cos(\alpha) + \sin(\alpha)\cos(\phi) + \cot(\mu)\sin(\phi) = 0$$

where θ is the Bragg angle (11.35 degrees for light of wavelength 1.54 angstroms), μ is the MFA, α is 90 degrees plus the rotation of the "front" face of the wood cell beyond perpendicular to the incoming beam, and ϕ is the azimuthal angle of the spot on the "2θ circle" on the back plane (measured counterclockwise from the east). See Figures 2 and 3.

In Figure 2, $\mathbf{b}$ denotes the direction vector for the microfibril. We have

$$\mathbf{b} = \begin{pmatrix} \sin(\mu)\cos(\alpha) \\ \sin(\mu)\sin(\alpha) \\ \cos(\mu) \end{pmatrix}.$$

Now there are two conditions that a 002 reflecting plane must meet to reflect a beam coming in along the x axis. First, $\mathbf{b}$ is in the 002 crystallographic planes of the cellulose crystals associated with the microfibrils so the normal, $\mathbf{p}$, to the 002 plane that succeeds in reflecting the beam must be perpendicular to $\mathbf{b}$. Second (the Bragg condition), the normal to the 002 reflecting plane must make a $90 - \theta$ angle to the x axis, where θ is the Bragg angle for the X-ray wavelength being used. Given these two conditions, we want to be able to determine the location at which the reflected beam intersects the back plane of the X-ray apparatus.

The first condition gives us

$$\mathbf{p} \cdot \mathbf{b} = 0$$

or

$$p_1 \sin(\mu)\cos(\alpha) + p_2 \sin(\mu)\sin(\alpha) + p_3 \cos(\mu) = 0. \tag{6}$$

The second condition gives us

$$p_1 = \begin{pmatrix} 1 \\ 0 \\ 0 \end{pmatrix} \cdot \mathbf{p} = \cos(90 - \theta) = \sin(\theta). \tag{7}$$

Combining Equations (6) and (7), we see that the (p_2, p_3) points must lie on the line

$$p_3 = (-\sin(\theta)\sin(\mu)\cos(\alpha) - p_2 \sin(\mu)\sin(\alpha))/\cos(\mu). \tag{8}$$

We also have

$$p_1^2 + p_2^2 + p_3^2 = 1. \tag{9}$$

Making use of Equations (7) and (9), we obtain

$$p_2^2 + p_3^2 = \cos^2(\theta). \tag{10}$$

Thus the solutions for (p_2, p_3) will be the 0, 1, or 2 points represented by the intersection of line (8) with circle (10). Circle (10) has radius $\cos(\theta)$ and a point on circle (10) has form $(\cos(\phi)\cos(\theta), \sin(\phi)\cos(\theta))$ for some angle ϕ. Since (Equation (7)) $p_1 = \sin(\theta)$ and $(p_2, p_3) = (\cos(\phi)\cos(\theta), \sin(\phi)\cos(\theta))$, we have

$$\begin{aligned} p_1 &= \sin(\theta) \\ p_2 &= \cos(\phi)\cos(\theta) \\ p_3 &= \sin(\phi)\cos(\theta) \end{aligned} \tag{11}$$

In section 6.3 we show that we can solve for ϕ (solve for the points of intersection of the line and the circle) by solving a quadratic equation.

Combining Equations (6) and (11) we obtain

$$\sin(\theta)\sin(\mu)\cos(\alpha) + \cos(\phi)\cos(\theta)\sin(\mu)\sin(\alpha) + \sin(\phi)\cos(\theta)\cos(\mu) = 0.$$

Dividing by $\cos(\theta)\sin(\mu)$ we obtain Cave's equation

$$\tan(\theta)\cos(\alpha) + \sin(\alpha)\cos(\phi) + \cot(\mu)\sin(\phi) = 0$$

where ϕ is related to $\mathbf{p}$ by (11), and we have not yet established a relation between ϕ and the azimuthal angle on the back plane.

6.2 Relation Between ϕ and the Azimuthal Angle on the Back Plane

Let us now consider the issue of where the reflected beam intersects the back plane. We know that the beam comes in along the x axis and reflects off a plane whose normal is given by (11). Consider now a canonical situation in which a beam reflects off a plane with normal (0,0,1) (the z axis). In this case the direction vector of the reflected beam is the same as the direction vector of the incident beam except that the sign of the z coordinate is reversed.

To make use of this result, we first find the transform that takes the $\mathbf{p}$ vector to the z vector. This requires a rotation of $90 - \phi$ degrees of the z axis towards the y axis (to bring the z axis in line with the projection of $\mathbf{p}$ onto the y, z plane), followed by a rotation of θ degrees of the z axis towards the x axis (to bring the z axis into line with $\mathbf{p}$). These two rotations can be represented by the transform

$$T \equiv \begin{pmatrix} \cos(\theta) & 0 & -\sin(\theta) \\ 0 & 1 & 0 \\ \sin(\theta) & 0 & \cos(\theta) \end{pmatrix} \begin{pmatrix} 1 & 0 & 0 \\ 0 & \sin(\phi) & -\cos(\phi) \\ 0 & \cos(\phi) & \sin(\phi) \end{pmatrix}.$$

One can check that

$$T(\mathbf{p}) = T \cdot \begin{pmatrix} \sin(\theta) \\ \cos(\phi)\cos(\theta) \\ \sin(\phi)\cos(\theta) \end{pmatrix} = \begin{pmatrix} 0 \\ 0 \\ 1 \end{pmatrix}.$$

Now in the original coordinate system, the X-ray incident direction is

$$\begin{pmatrix} -1 \\ 0 \\ 0 \end{pmatrix}.$$

In the coordinate system in which the $\mathbf{p}$ vector has been transformed to the z vector, this incident direction becomes

$$T \cdot \begin{pmatrix} -1 \\ 0 \\ 0 \end{pmatrix} = \begin{pmatrix} -\cos(\theta) \\ 0 \\ -\sin(\theta) \end{pmatrix}$$

so the beam reflects off in the

$$\begin{pmatrix} -\cos(\theta) \\ 0 \\ \sin(\theta) \end{pmatrix}$$

direction. Transformed back into the original coordinate system, this direction vector is

$$\begin{pmatrix} 1 & 0 & 0 \\ 0 & \sin(\phi) & -\cos(\phi) \\ 0 & \cos(\phi) & \sin(\phi) \end{pmatrix}^{-1} \begin{pmatrix} \cos(\theta) & 0 & -\sin(\theta) \\ 0 & 1 & 0 \\ \sin(\theta) & 0 & \cos(\theta) \end{pmatrix}^{-1} \begin{pmatrix} -\cos(\theta) \\ 0 \\ \sin(\theta) \end{pmatrix}$$

$$= \begin{pmatrix} -\cos(2\theta) \\ \cos(\phi)\sin(2\theta) \\ \sin(\phi)\sin(2\theta) \end{pmatrix}.$$

We extend a beam in this direction to its intersection with a back plane that is perpendicular to the x axis and x_0 units behind the specimen by multiplying by a factor of $x_0/\cos(2\theta)$. Thus the beam intersects the back plane at the point

$$\begin{pmatrix} -x_0 \\ \cos(\phi)\sin(2\theta)x_0/(\cos(2\theta)) \\ \sin(\phi)\sin(2\theta)x_0/(\cos(2\theta)) \end{pmatrix} = \begin{pmatrix} -x_0 \\ \cos(\phi)\tan(2\theta)x_0 \\ \sin(\phi)\tan(2\theta)x_0 \end{pmatrix}.$$

Looking face on at the back plane, this is the point that is on the circle of radius $\tan(2\theta)x_0$ (the "2θ circle") and ϕ degrees in a counterclockwise direction from the y axis. So the ϕ that is a solution to (11) is also the azimuthal angle of the point of maximum X-ray intensity.

6.3 Solution of Cave's Equation

Given values for θ, α, and μ, we can use a nonlinear equation solver to find values for ϕ (this is the method that was used to create Figures 4 – 16), but we can also transform the equation into a quadratic equation. Consider the equation

$$\tan(\theta)\cos(\alpha) + \cos(\phi)\sin(\alpha) + \sqrt{1-\cos^2(\phi)}\cot(\mu) = 0 \tag{12}$$

for $\phi \in [0, \pi]$. This becomes

$$\sin^2(\alpha)\cos^2(\phi) + 2\tan(\theta)\cos(\alpha)\sin(\alpha)\cos(\phi) + \tan^2(\theta)\cos^2(\alpha) \tag{13}$$

$$= (1-\cos^2(\phi))\cot^2(\mu)$$

or

$$a\cos^2(\phi) + b\cos(\phi) + c = 0$$

where

$$\begin{aligned} a &= \sin^2(\alpha) + \cot^2(\mu), \\ b &= \tan(\theta)\sin(2\alpha), \end{aligned}$$

and

$$c = \tan^2(\theta)\cos^2(\alpha) - \cot^2(\mu).$$

We can of course then solve for $\cos(\phi)$ via the quadratic formula:

$$\left(-b \pm \sqrt{b^2 - 4ac}\right)/(2a).$$

Obviously, if $a = \sin^2(\alpha) + \cot^2(\mu)$ equals 0, then this approach does not work, so we will assume in what follows that $a > 0$.

To show that two distinct solutions exist, we need to establish that $b^2 - 4ac > 0$. Since $a > 0$, this will follow if $c < 0$. It is clear that $c < 0$ if $\mu < 90 - \theta$. For our experimental apparatus $\theta = 11.35$ degrees so $b^2 - 4ac$ will be positive for MFAs less than 78.65 degrees. In what follows we will assume that $\mu < 90 - \theta$.

In addition to showing that solutions exist, we also want to show that they lie in [-1,1] so that we can take the inverse cosine of these values to obtain ϕ values.

First let us demonstrate that

$$\left(-b \pm \sqrt{b^2 - 4ac}\right)/(2a) \leq 1. \tag{14}$$

It is clear that result (14) follows if

$$b + 2a \geq \pm\sqrt{b^2 - 4ac} \tag{15}$$

To proceed we first need to establish that $b + 2a \geq 0$. Since we are assuming that $\mu < 90 - \theta$, we have

$$\begin{aligned} b + 2a &= \tan(\theta)2\sin(\alpha)\cos(\alpha) + 2\sin^2(\alpha) + 2\cot^2(\mu) \\ &\geq 2(\tan(\theta)\sin(\alpha)\cos(\alpha) + \sin^2(\alpha) + \tan^2(\theta)). \end{aligned} \tag{16}$$

If $\sin(\alpha) \geq 0$, the quantity on the right in Equation (16) is greater than or equal to

$$2(\sin^2(\alpha) - 2\tan(\theta)\sin(\alpha) + \tan^2(\theta)) = (\sin(\alpha) - \tan(\theta))^2 \geq 0.$$

If $\sin(\alpha) \leq 0$, the quantity on the right in Equation (16) is greater than or equal to

$$2(\sin^2(\alpha) + 2\tan(\theta)\sin(\alpha) + \tan^2(\theta)) = (\sin(\alpha) + \tan(\theta))^2 \geq 0.$$

Thus we do have

$$b + 2a \geq 0. \tag{17}$$

Since result (17) holds, result (15) will follow if we can show that

$$b^2 + 4ab + 4a^2 = (b + 2a)^2 \geq b^2 - 4ac. \tag{18}$$

This will follow if we can show that (recall that we are assuming that $a > 0$)

$$b + a \geq -c$$

or

$$\tan(\theta)\sin(2\alpha) + \sin^2(\alpha) + \cot^2(\mu) \geq -(\tan^2(\theta)\cos^2(\alpha) - \cot^2(\mu))$$

or

$$2\tan(\theta)\sin(\alpha)\cos(\alpha) + \sin^2(\alpha) + \tan^2(\theta)\cos^2(\alpha) \geq 0. \tag{19}$$

But

$$2\tan(\theta)\sin(\alpha)\cos(\alpha) + \sin^2(\alpha) + \tan^2(\theta)\cos^2(\alpha) = (\sin(\alpha) + \tan(\theta)\cos(\alpha))^2 \geq 0$$

so result (19) does indeed hold, which establishes result (14).

A similar chain of reasoning establishes that

$$\left(-b \pm \sqrt{b^2 - 4ac}\right)/(2a) \geq -1. \tag{20}$$

Thus the quadratic equation (13) leads to two distinct ϕs in $[0, \pi]$.

The equation

$$\tan(\theta)\cos(\alpha) + \cos(\phi)\sin(\alpha) - \sqrt{1 - \cos^2(\phi)}\cot(\mu) = 0 \tag{21}$$

for $\phi \in [-\pi, 0]$ again becomes

$$\sin^2(\alpha)\cos^2(\phi) + 2\tan(\theta)\cos(\alpha)\sin(\alpha)\cos(\phi) + \tan^2(\theta)\cos^2(\alpha)$$

$$= (1 - \cos^2(\phi))\cot^2(\mu)$$

so the solutions of (21) are simply the negations of the solutions of (12).

Now note that if ϕ is a solution of Cave's original equation

$$\tan(\theta)\cos(\alpha) + \sin(\alpha)\cos(\phi) + \cot(\mu)\sin(\phi) = 0$$

then $-\phi$ is a solution of

$$\tan(\theta)\cos(\alpha + \pi) = \sin(\alpha + \pi)\cos(\phi) + \cot(\mu)\sin(\phi) = 0.$$

Thus the four ϕ associated with the two opposite sides of a square cell can be found by obtaining the two distinct solutions to the quadratic equation (13) and then negating them. (The two solutions to (13) will often correspond to two opposite faces of the cell. See Figures 4 – 16.) This is the approach that we take in our computer program.

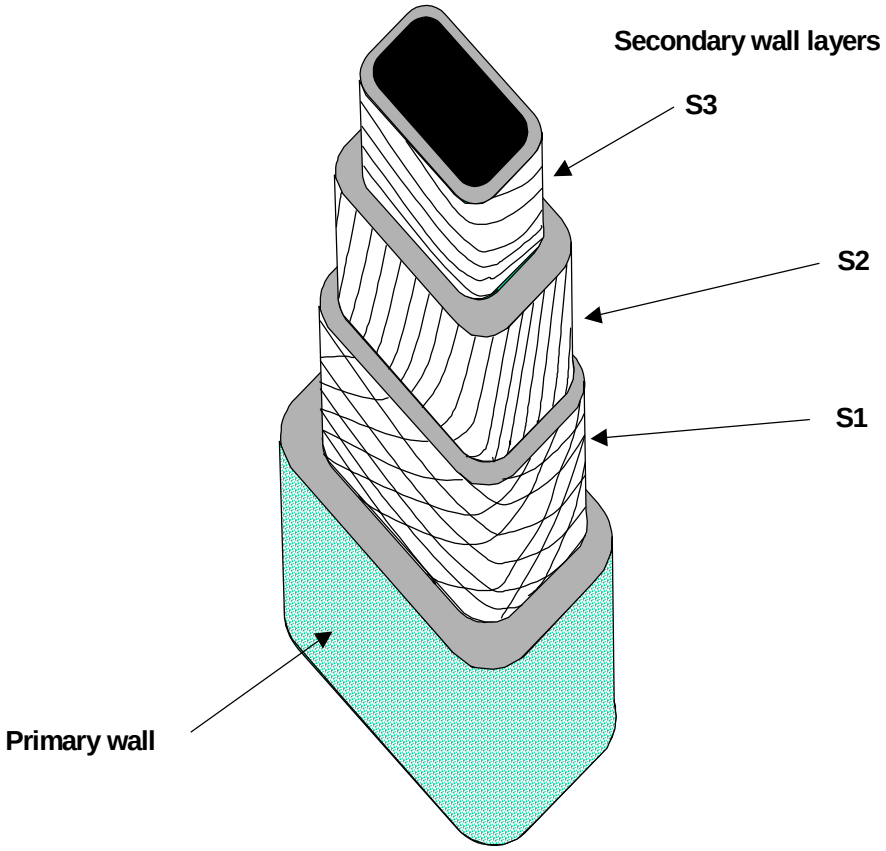

Figure 1: Wood cell structure

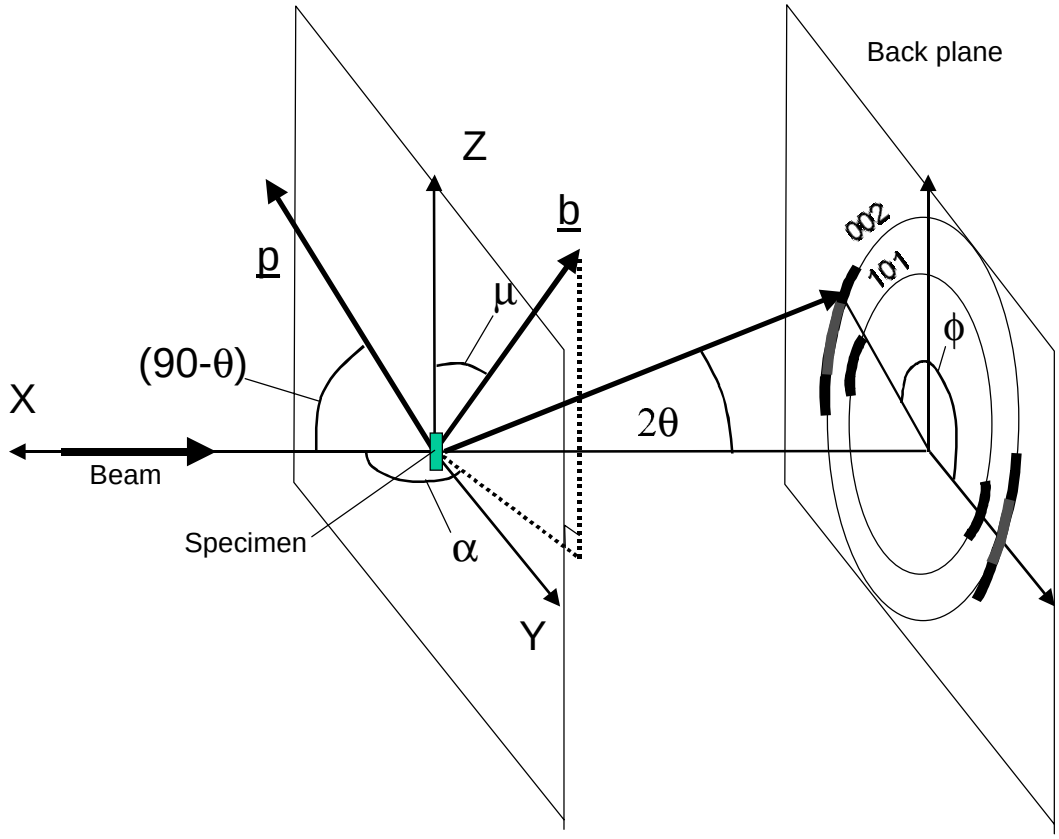

Figure 2: Geometry of the X-ray diffraction

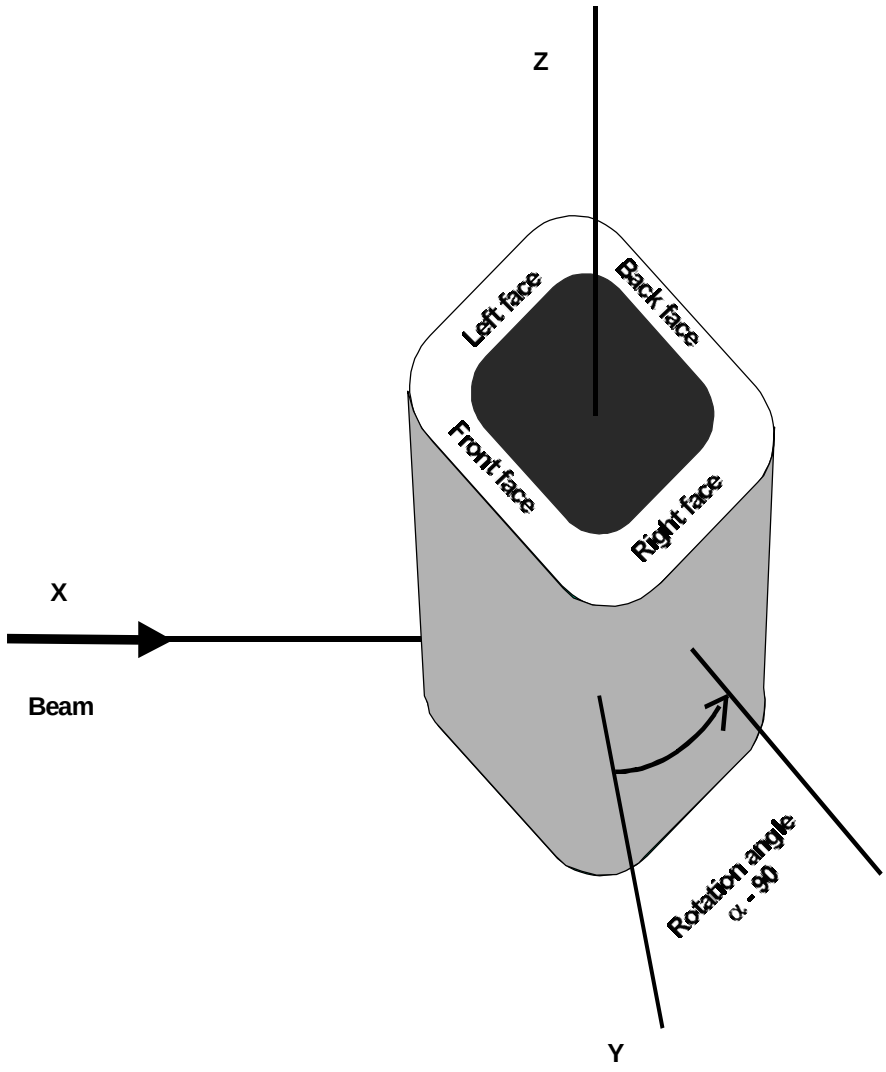

Figure 3: Wood cell rotation

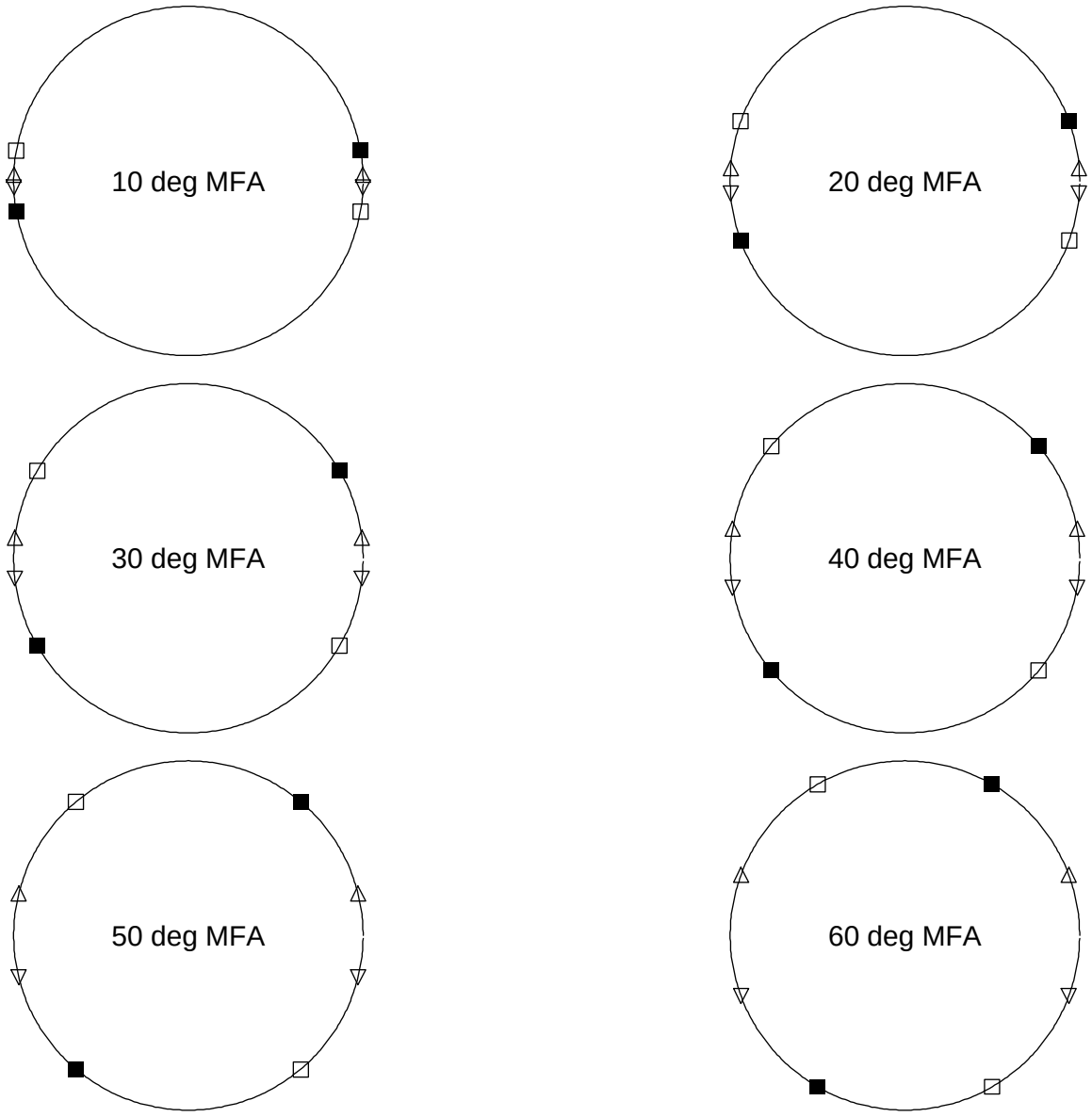

Figure 4: Locations of high intensity X-ray spots on the back plane for **wood cell rotation = 0 degrees**

□ — spots due to the **front** (before rotation) face
■ — spots due to the **back** face
△ — spots due to the **right** face
▽ — spots due to the **left** face

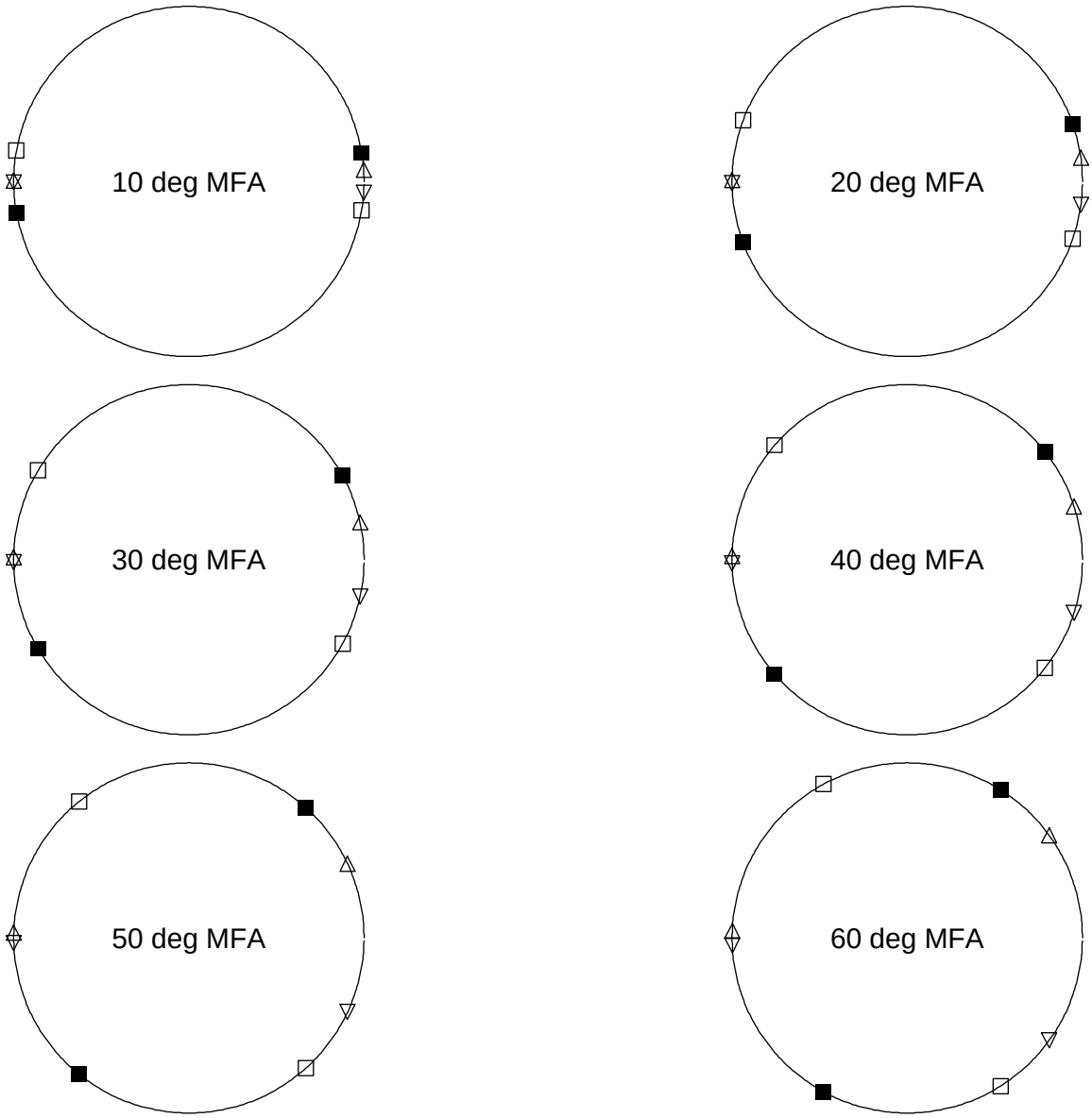

Figure 5: Locations of high intensity X-ray spots on the back plane for **wood cell rotation = 10 degrees**

□ — spots due to the **front** (before rotation) face
■ — spots due to the **back** face
△ — spots due to the **right** face
▽ — spots due to the **left** face

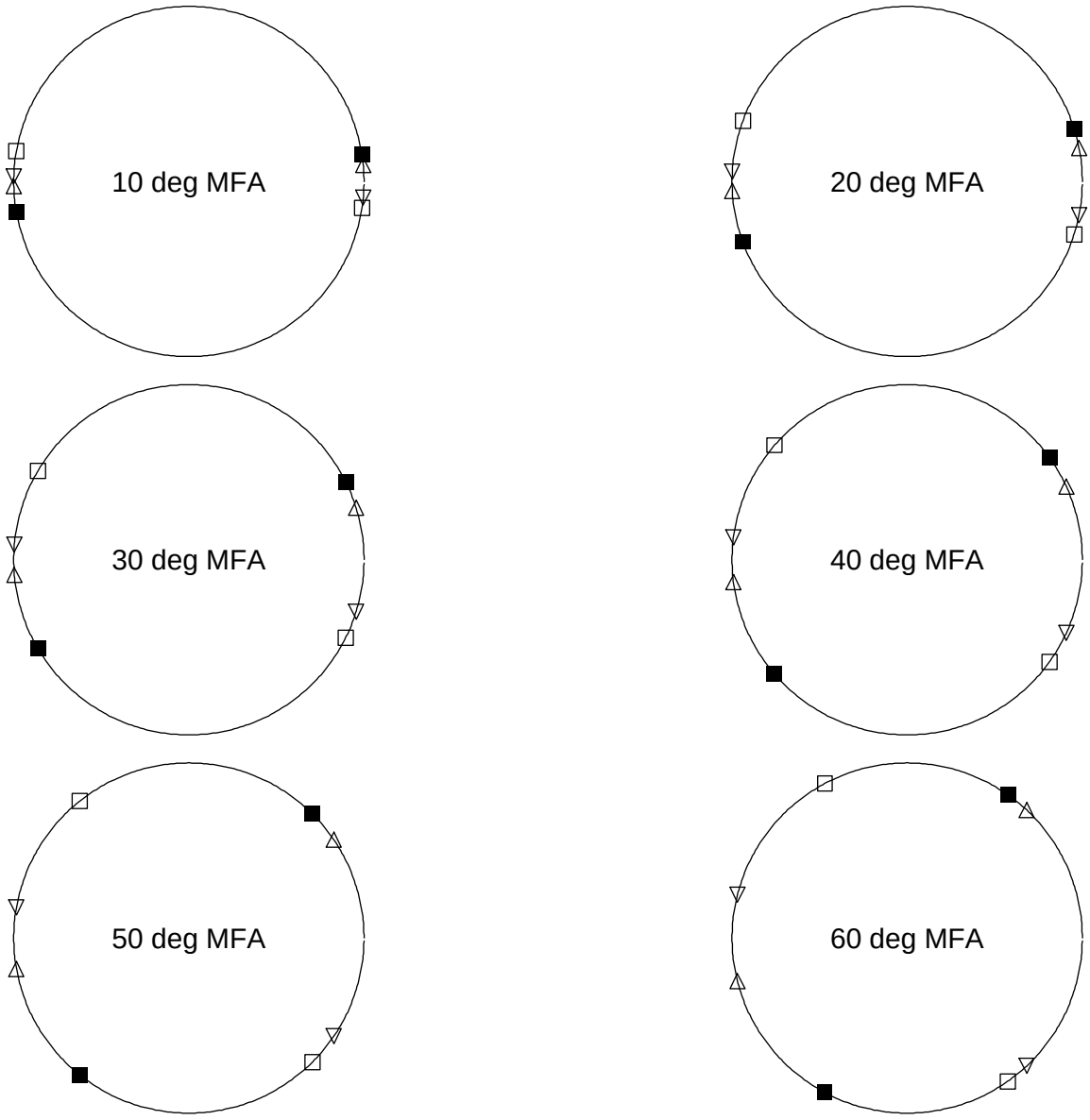

Figure 6: Locations of high intensity X-ray spots on the back plane for **wood cell rotation = 20 degrees**

□ — spots due to the **front** (before rotation) face
■ — spots due to the **back** face
△ — spots due to the **right** face
▽ — spots due to the **left** face

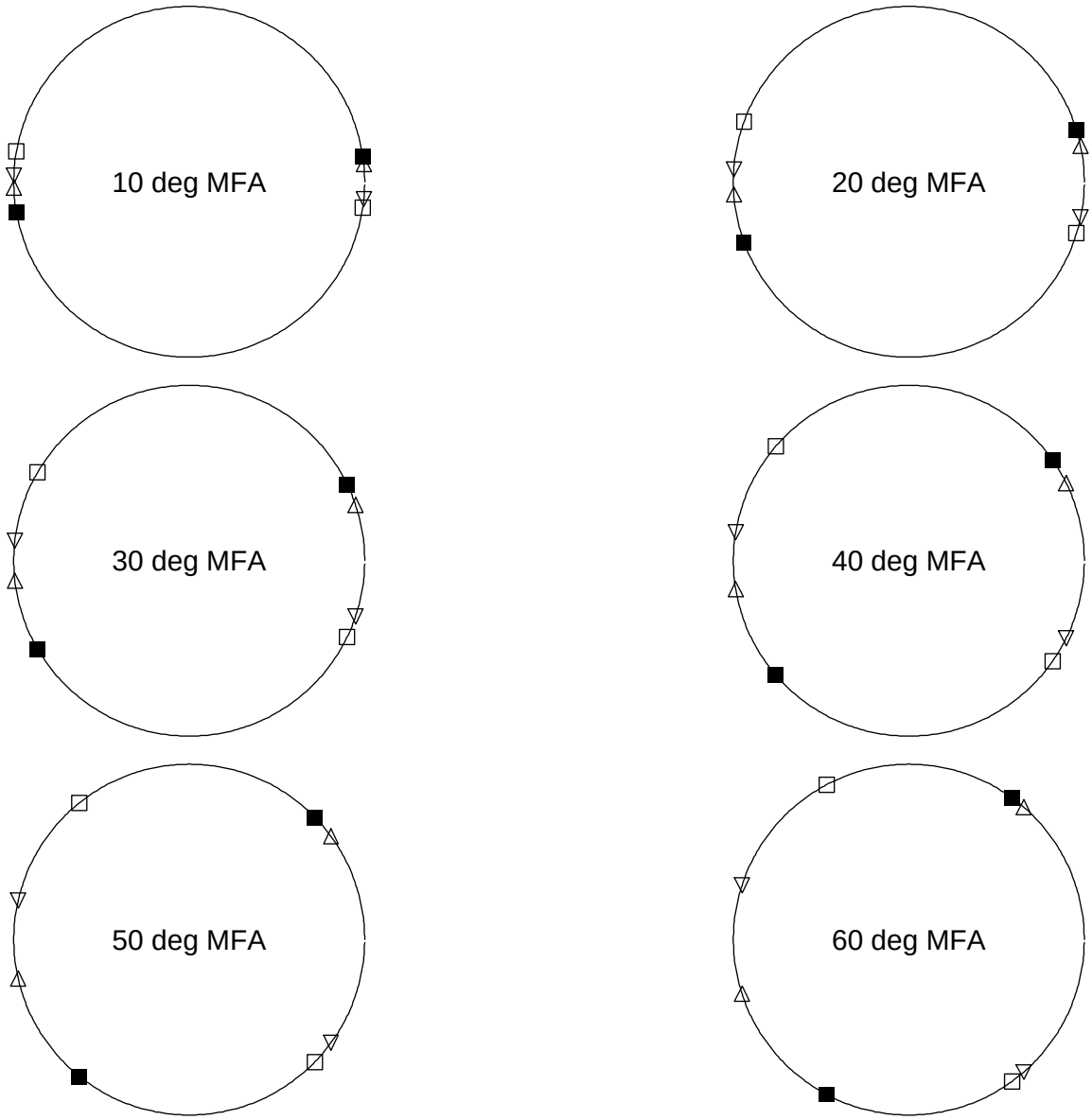

Figure 7: Locations of high intensity X-ray spots on the back plane for **wood cell rotation = 22.5 degrees**

□ — spots due to the **front** (before rotation) face
■ — spots due to the **back** face
△ — spots due to the **right** face
▽ — spots due to the **left** face

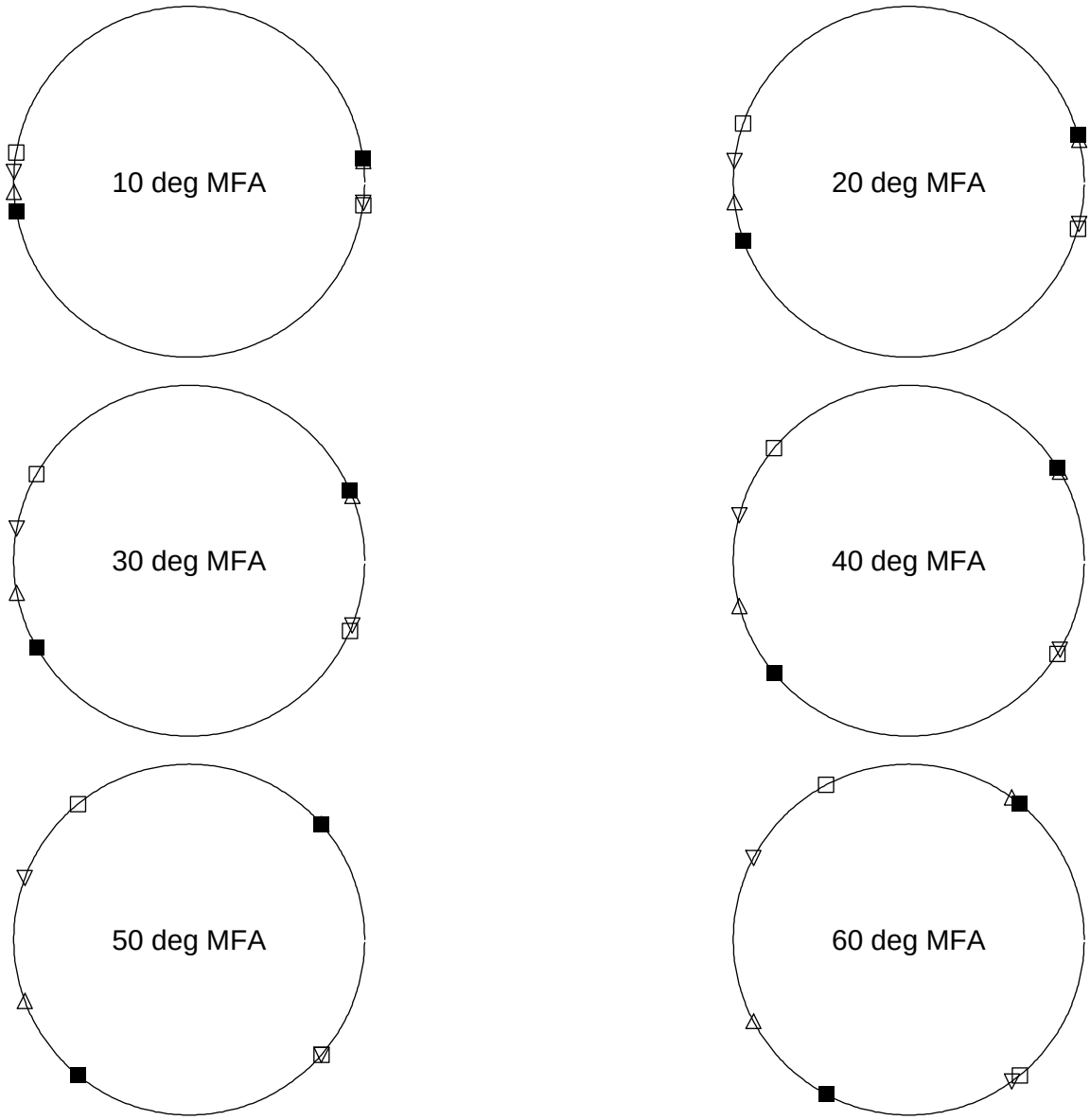

Figure 8: Locations of high intensity X-ray spots on the back plane for **wood cell rotation = 30 degrees**

□ — spots due to the **front** (before rotation) face
■ — spots due to the **back** face
△ — spots due to the **right** face
▽ — spots due to the **left** face

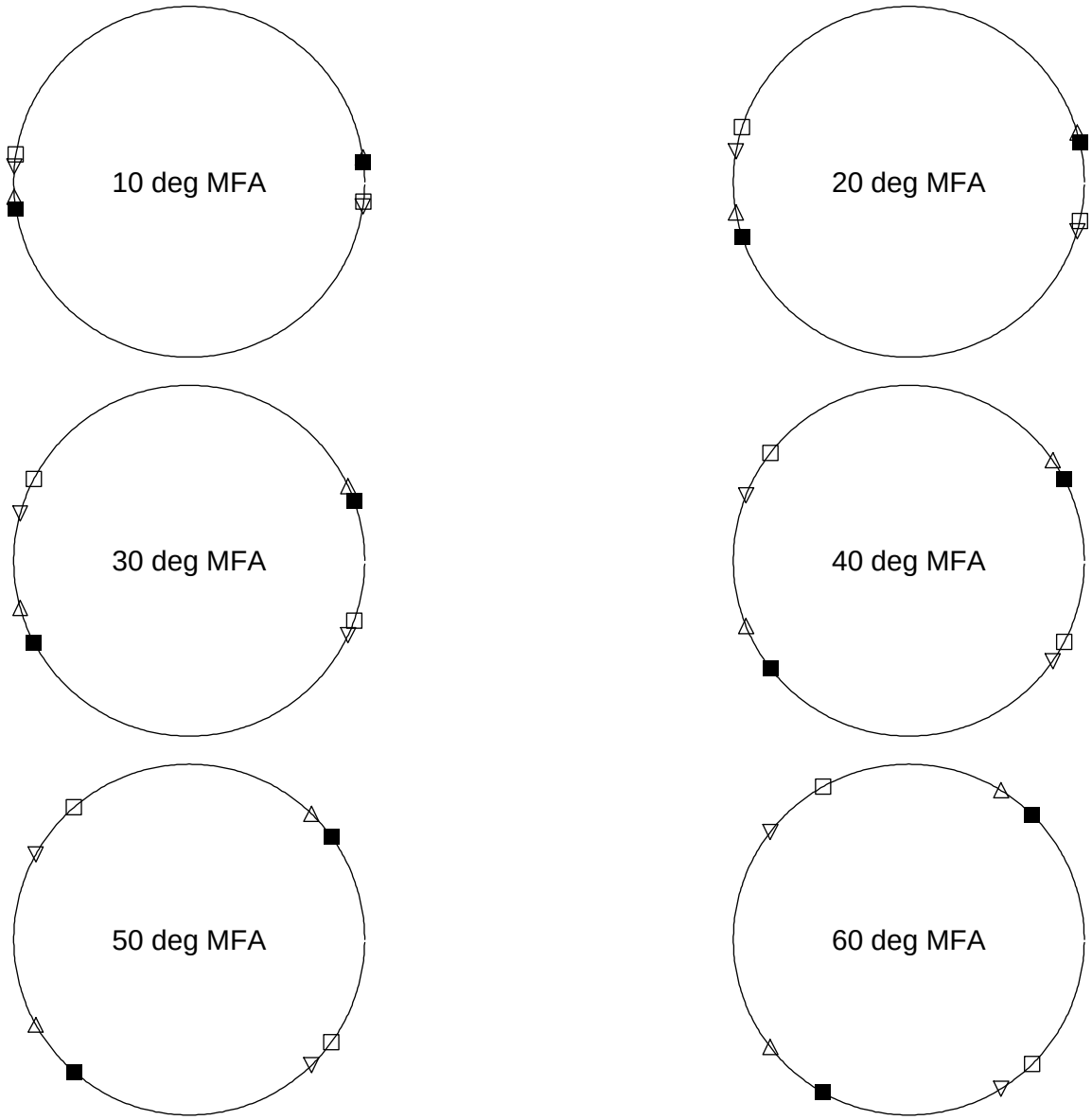

Figure 9: Locations of high intensity X-ray spots on the back plane for **wood cell rotation = 40 degrees**

□ — spots due to the **front** (before rotation) face
■ — spots due to the **back** face
△ — spots due to the **right** face
▽ — spots due to the **left** face

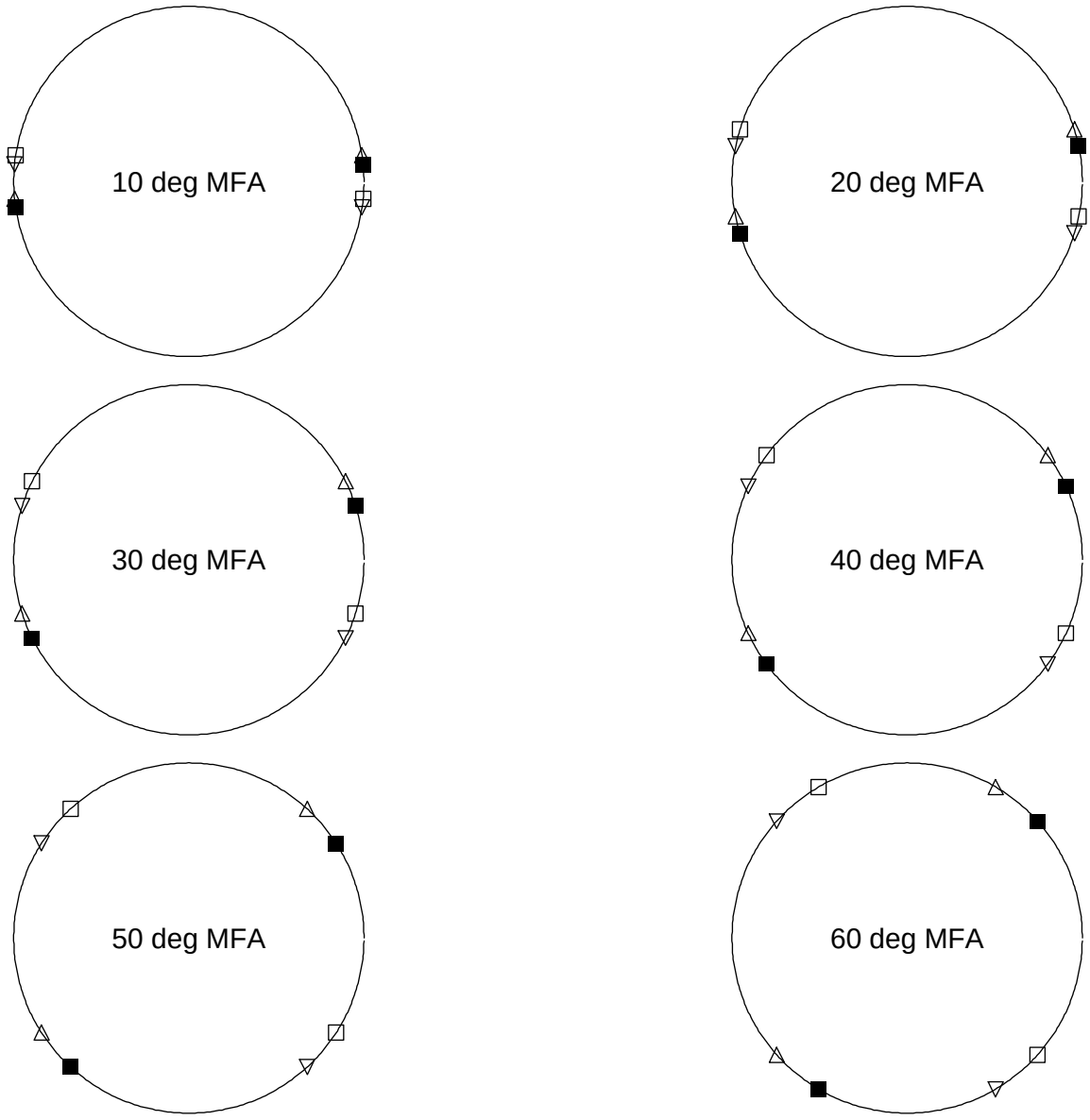

Figure 10: Locations of high intensity X-ray spots on the back plane for **wood cell rotation = 45 degrees**

□ — spots due to the **front** (before rotation) face
■ — spots due to the **back** face
△ — spots due to the **right** face
▽ — spots due to the **left** face

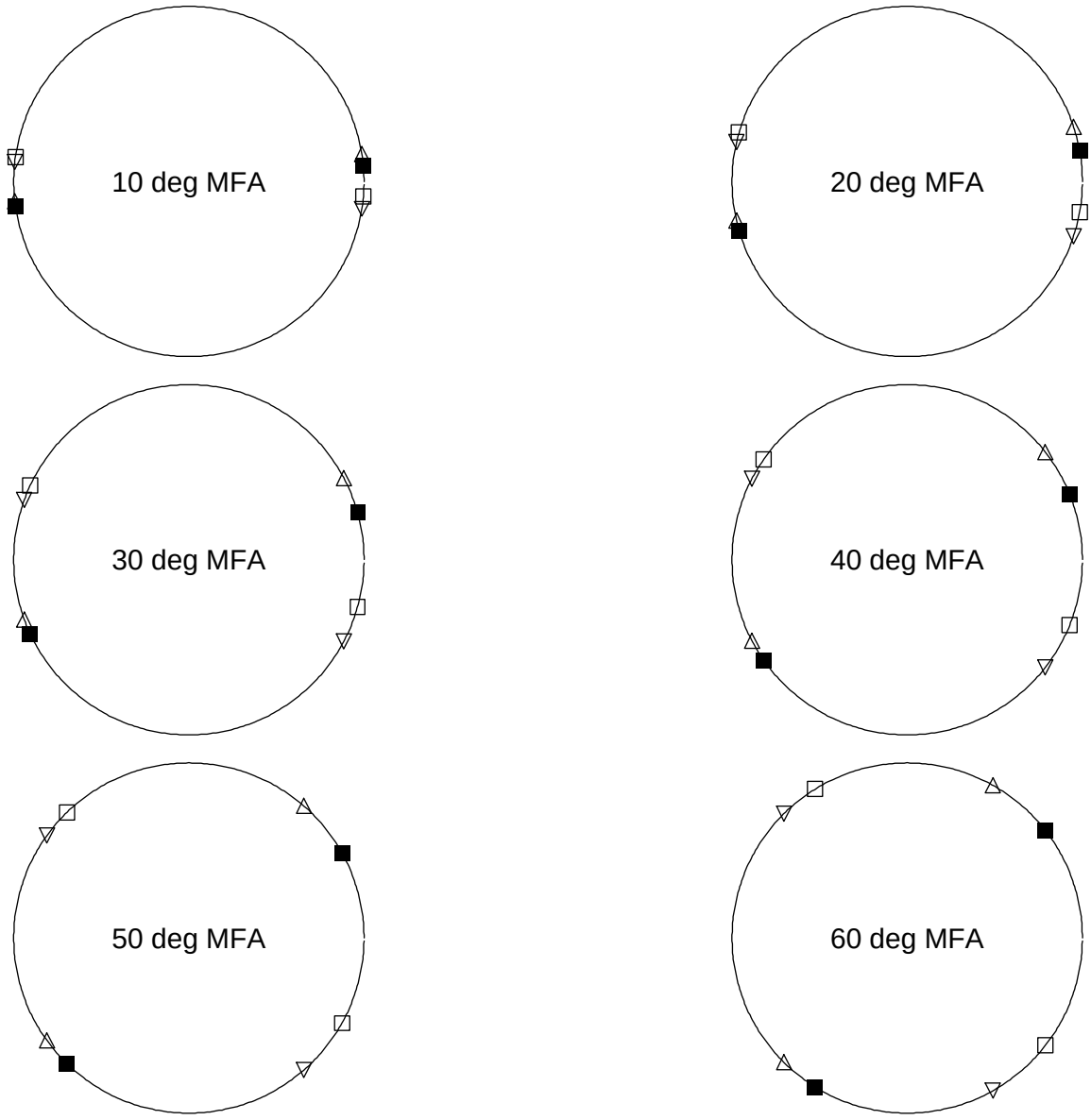

Figure 11: Locations of high intensity X-ray spots on the back plane for **wood cell rotation = 50 degrees**

□ — spots due to the **front** (before rotation) face
■ — spots due to the **back** face
△ — spots due to the **right** face
▽ — spots due to the **left** face

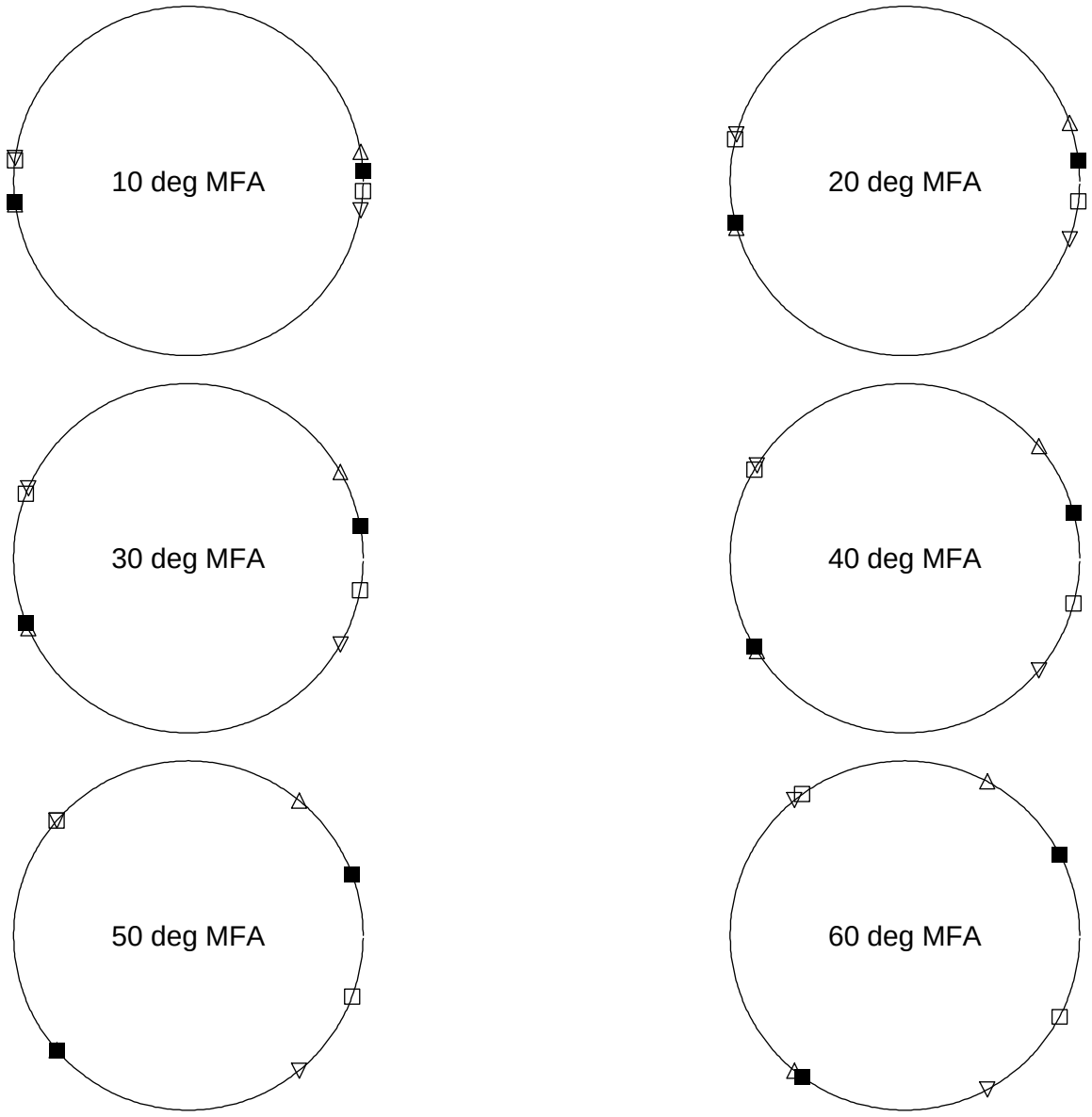

Figure 12: Locations of high intensity X-ray spots on the back plane for **wood cell rotation = 60 degrees**

□ — spots due to the **front** (before rotation) face
■ — spots due to the **back** face
△ — spots due to the **right** face
▽ — spots due to the **left** face

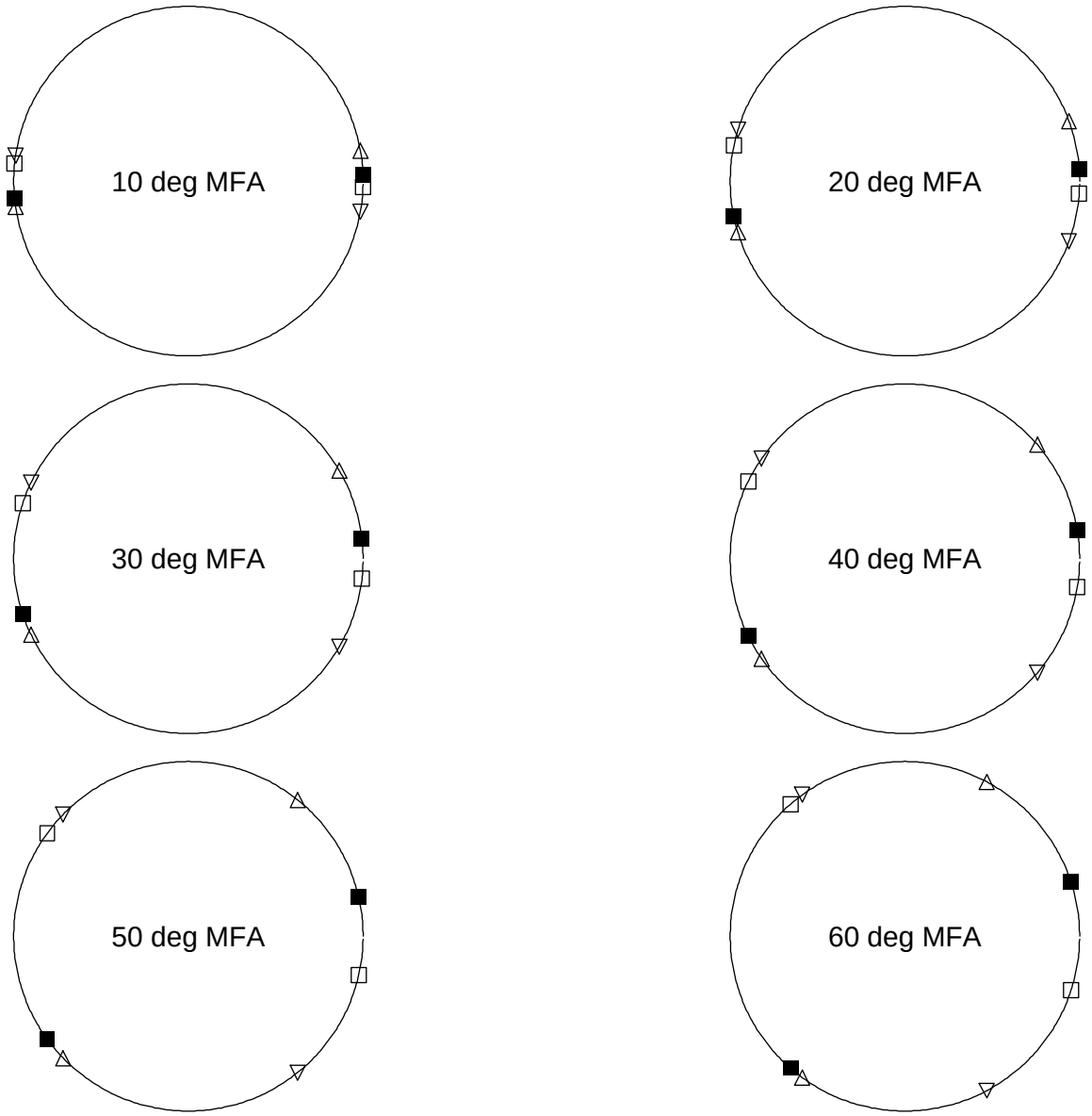

Figure 13: Locations of high intensity X-ray spots on the back plane for **wood cell rotation = 67.5 degrees**

□ — spots due to the **front** (before rotation) face
■ — spots due to the **back** face
△ — spots due to the **right** face
▽ — spots due to the **left** face

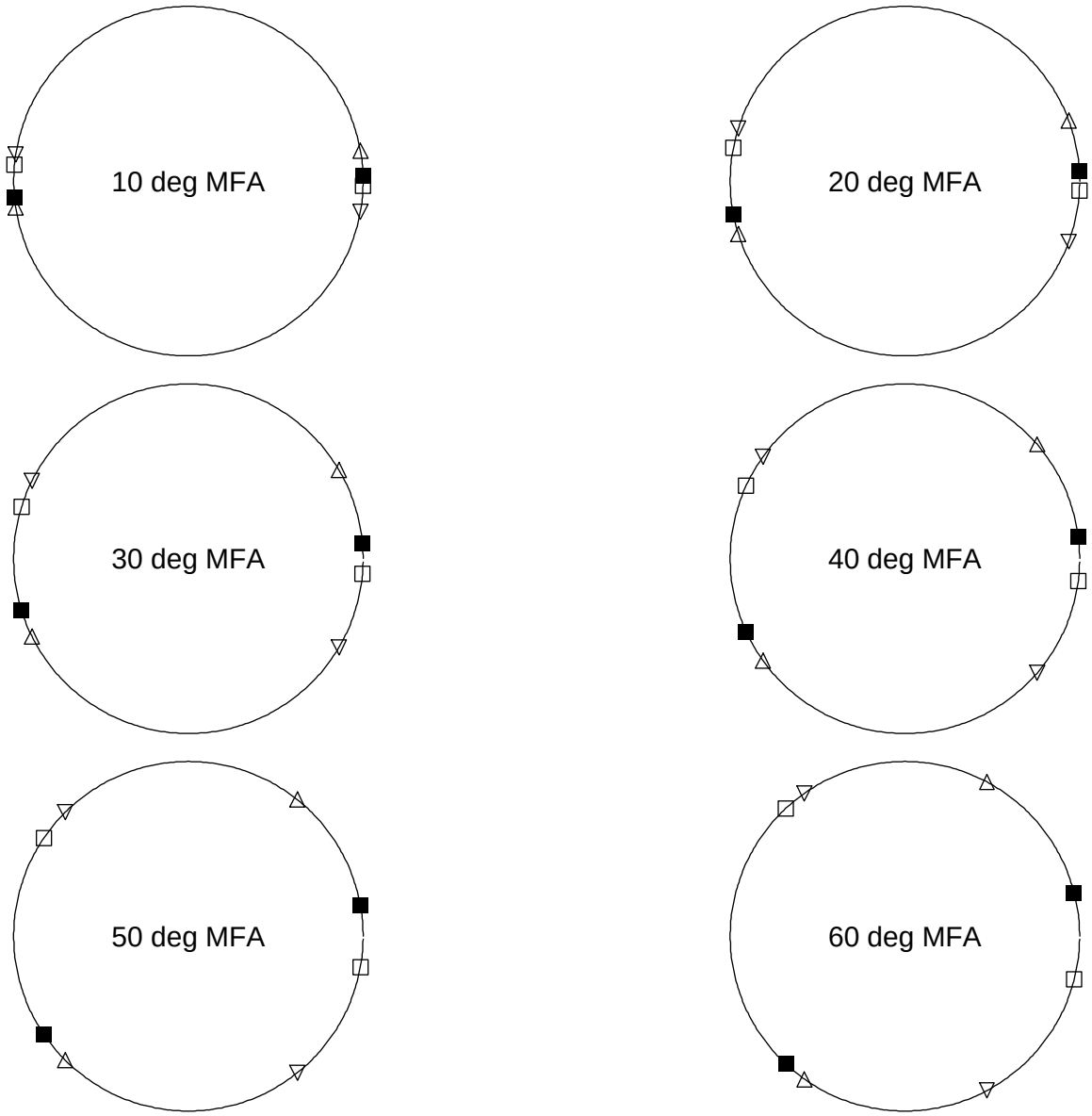

Figure 14: Locations of high intensity X-ray spots on the back plane for **wood cell rotation = 70 degrees**

□ — spots due to the **front** (before rotation) face
■ — spots due to the **back** face
△ — spots due to the **right** face
▽ — spots due to the **left** face

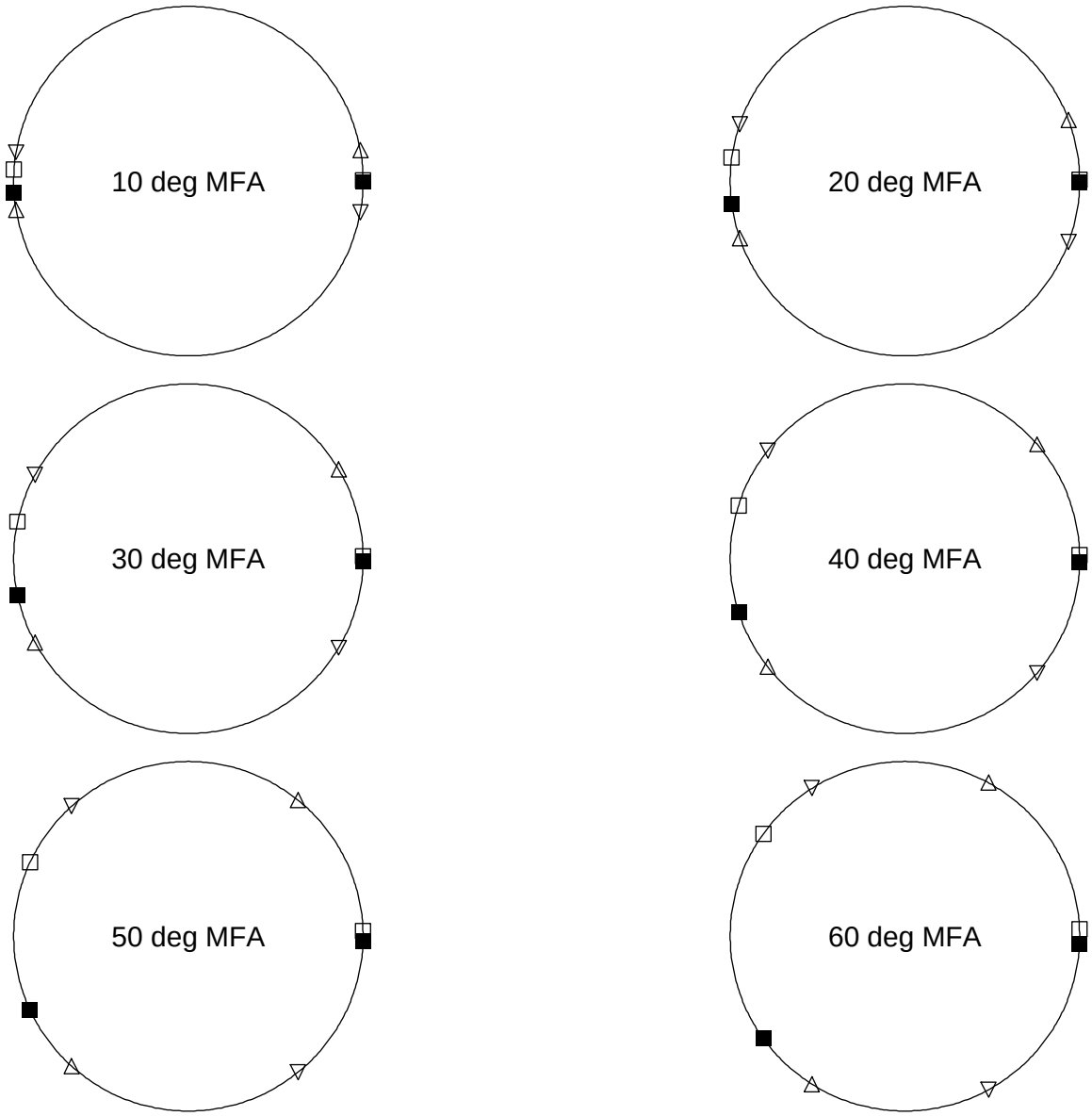

Figure 15: Locations of high intensity X-ray spots on the back plane for **wood cell rotation = 80 degrees**

□ — spots due to the **front** (before rotation) face
■ — spots due to the **back** face
△ — spots due to the **right** face
▽ — spots due to the **left** face

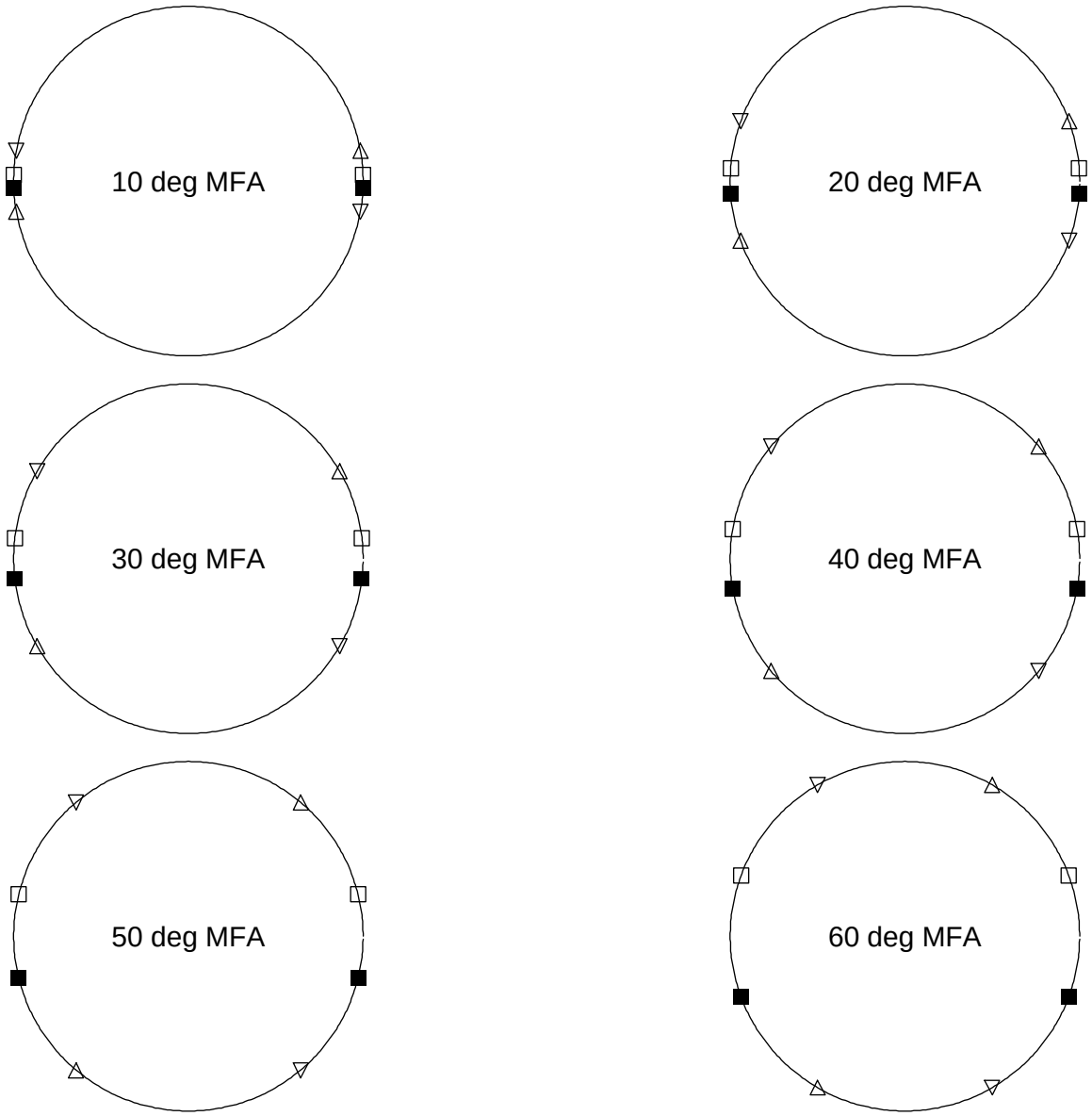

Figure 16: Locations of high intensity X-ray spots on the back plane for **wood cell rotation = 90 degrees**

□ — spots due to the **front** (before rotation) face
■ — spots due to the **back** face
△ — spots due to the **right** face
▽ — spots due to the **left** face

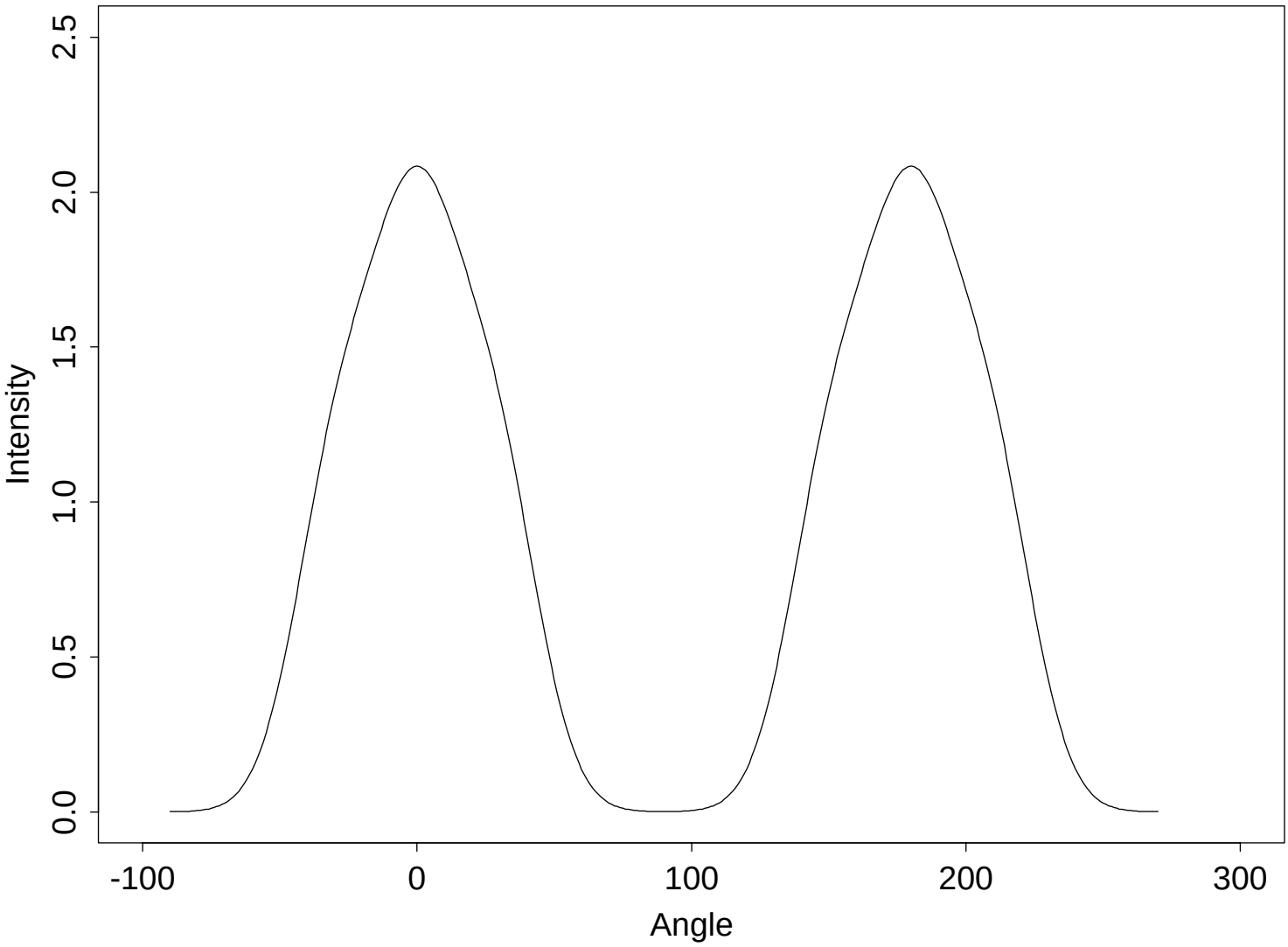

Figure 17: Calculated intensity profile for wood cell rotation = 0 degrees, microfibril angle = 30 degrees, broadening factor σ = 15 degrees

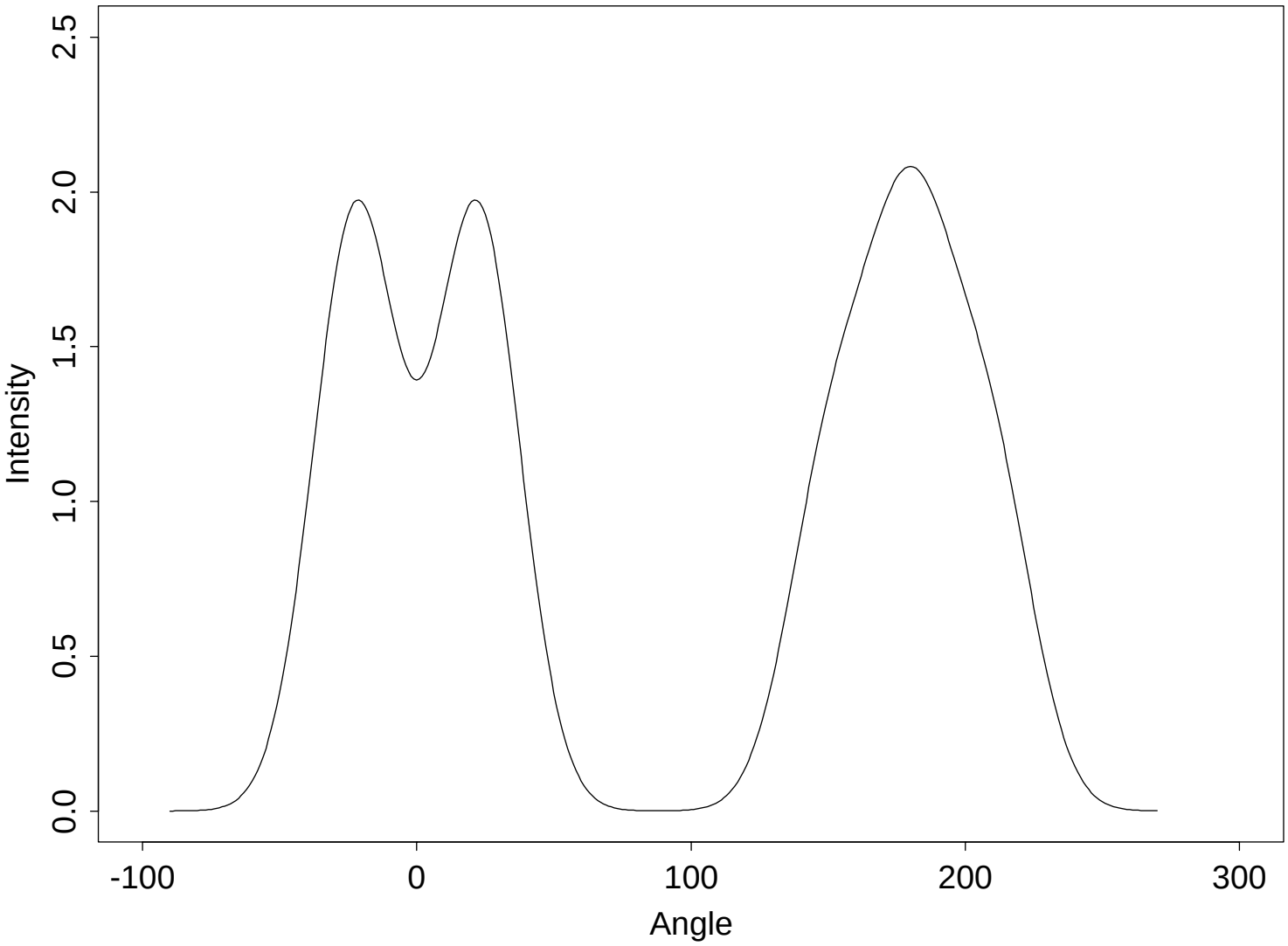

Figure 18: Calculated intensity profile for wood cell rotation = 22.5 degrees, microfibril angle = 30 degrees, broadening factor σ = 15 degrees

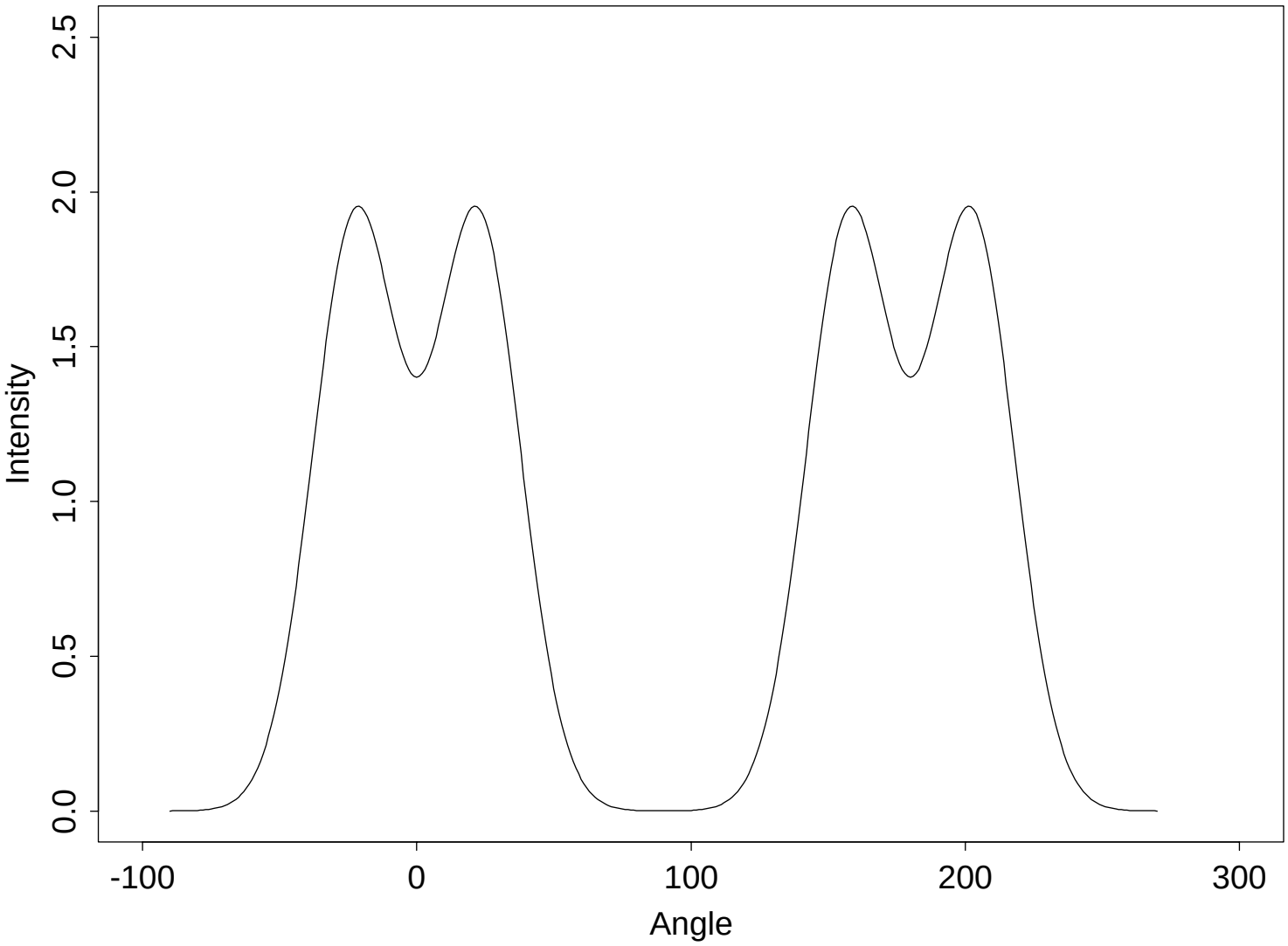

Figure 19: Calculated intensity profile for wood cell rotation = 45 degrees, microfibril angle = 30 degrees, broadening factor σ = 15 degrees

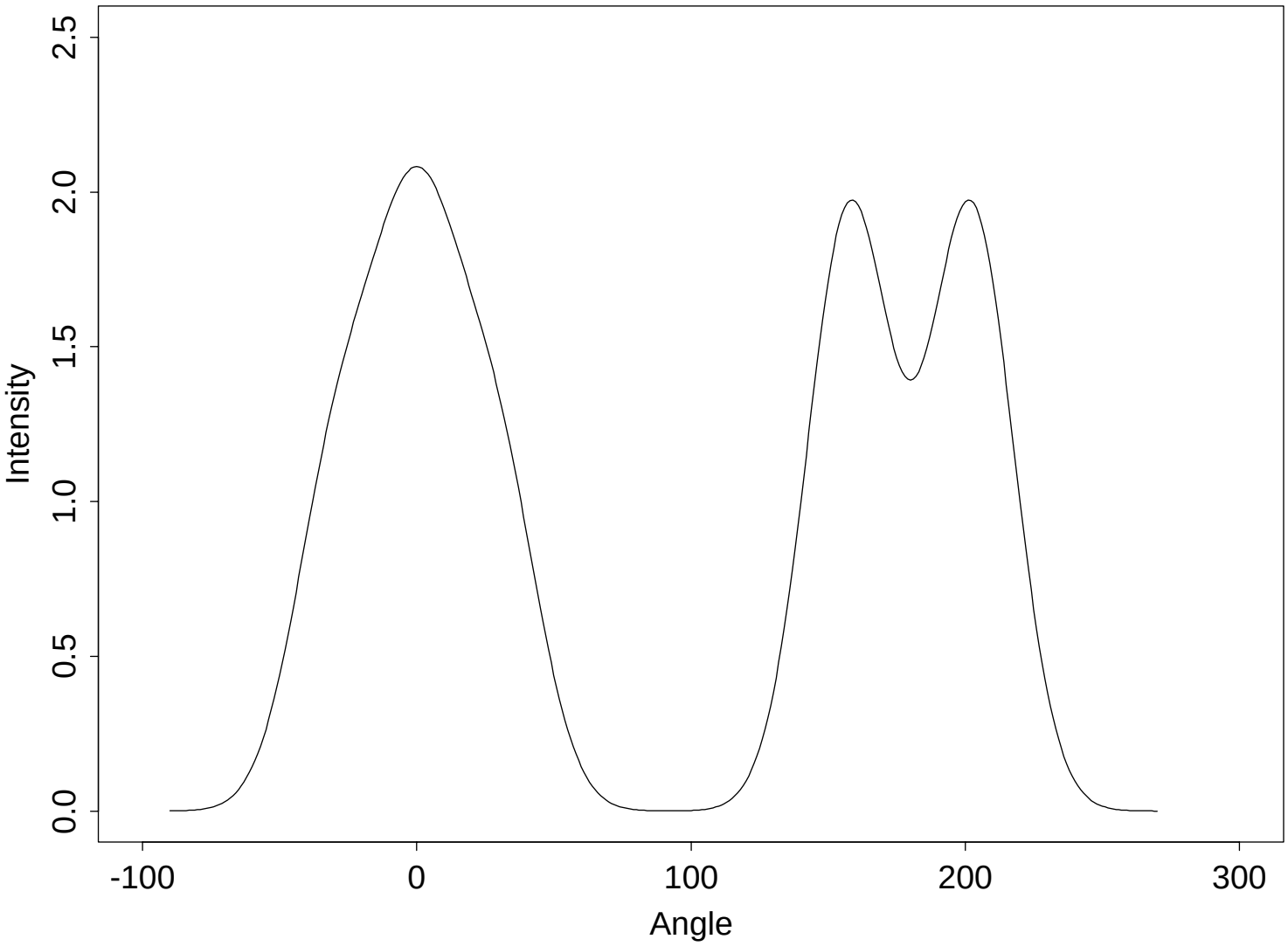

Figure 20: Calculated intensity profile for wood cell rotation = 67.5 (or -22.5) degrees, microfibril angle = 30 degrees, broadening factor σ = 15 degrees

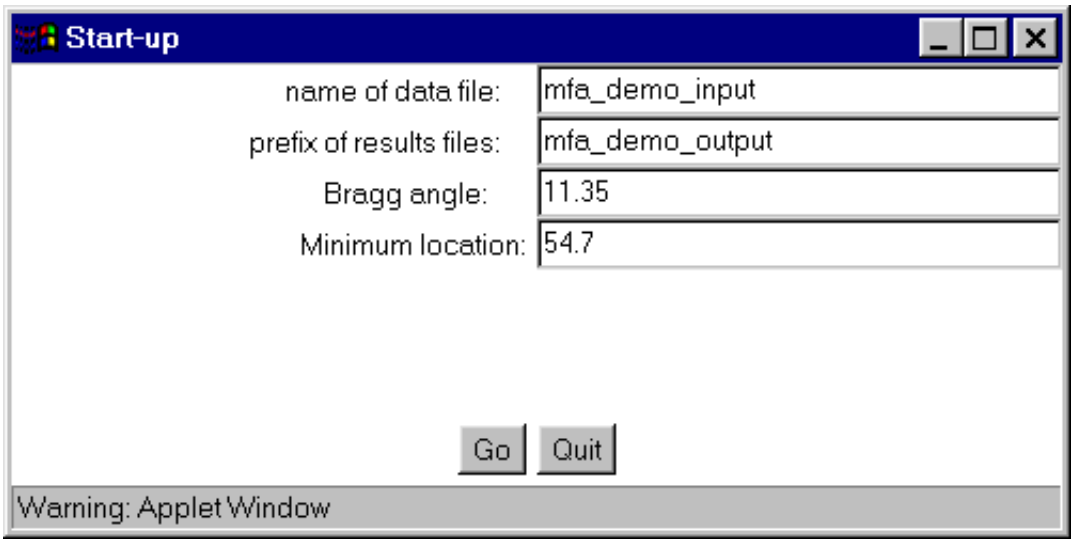

Figure 21: Start-up window for the applet

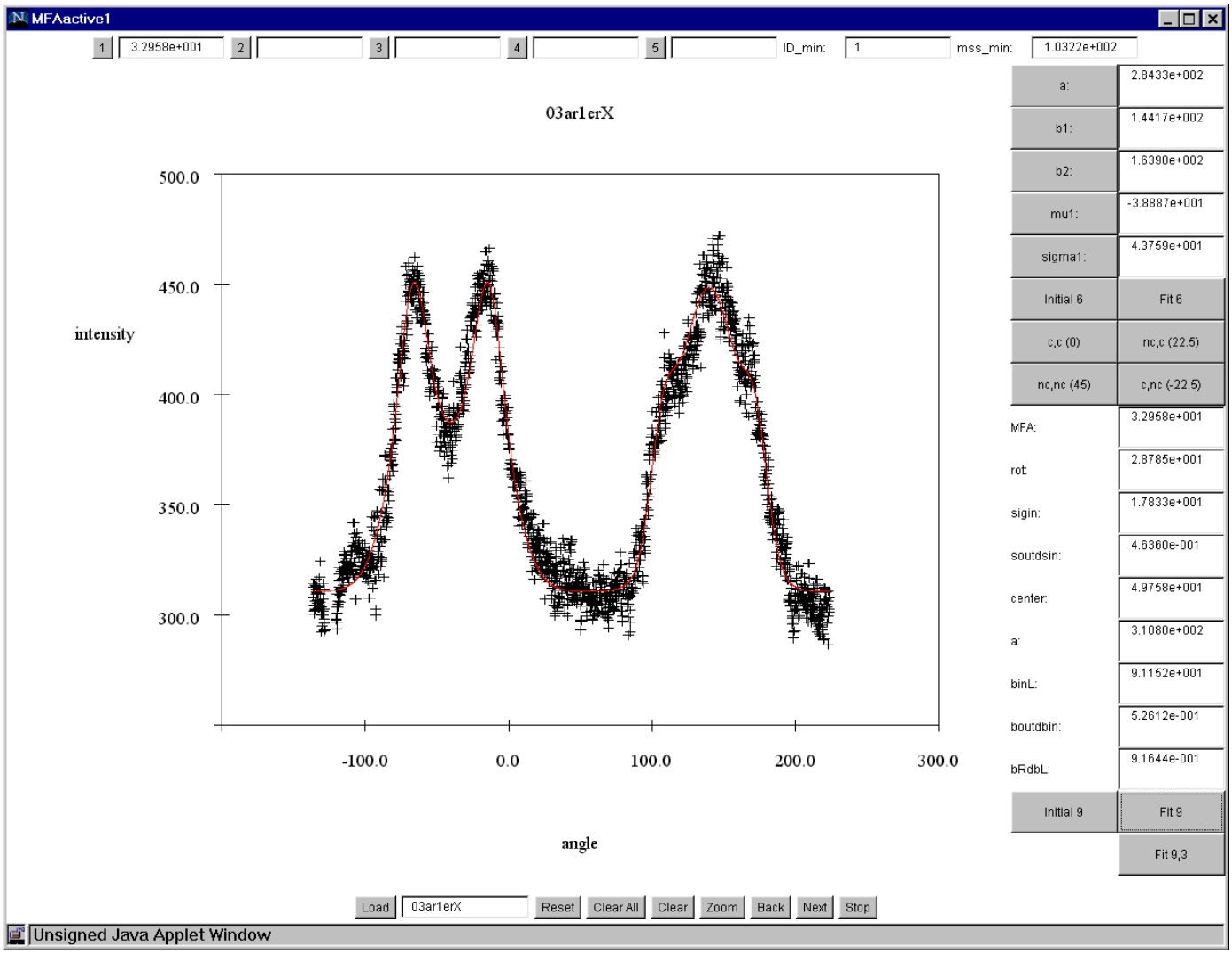

Figure 22: Main window for the applet

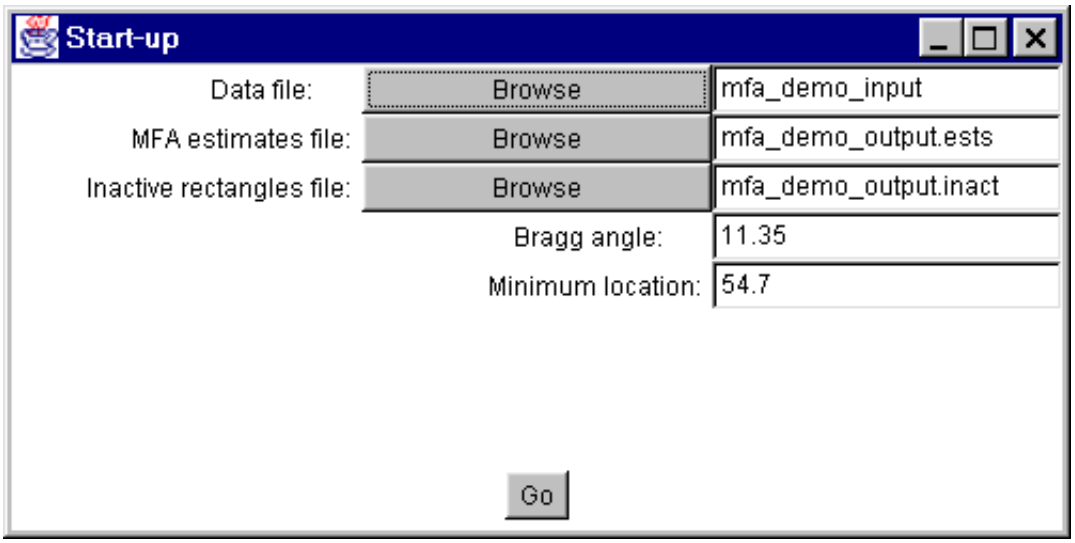

Figure 23: Start-up window for the application

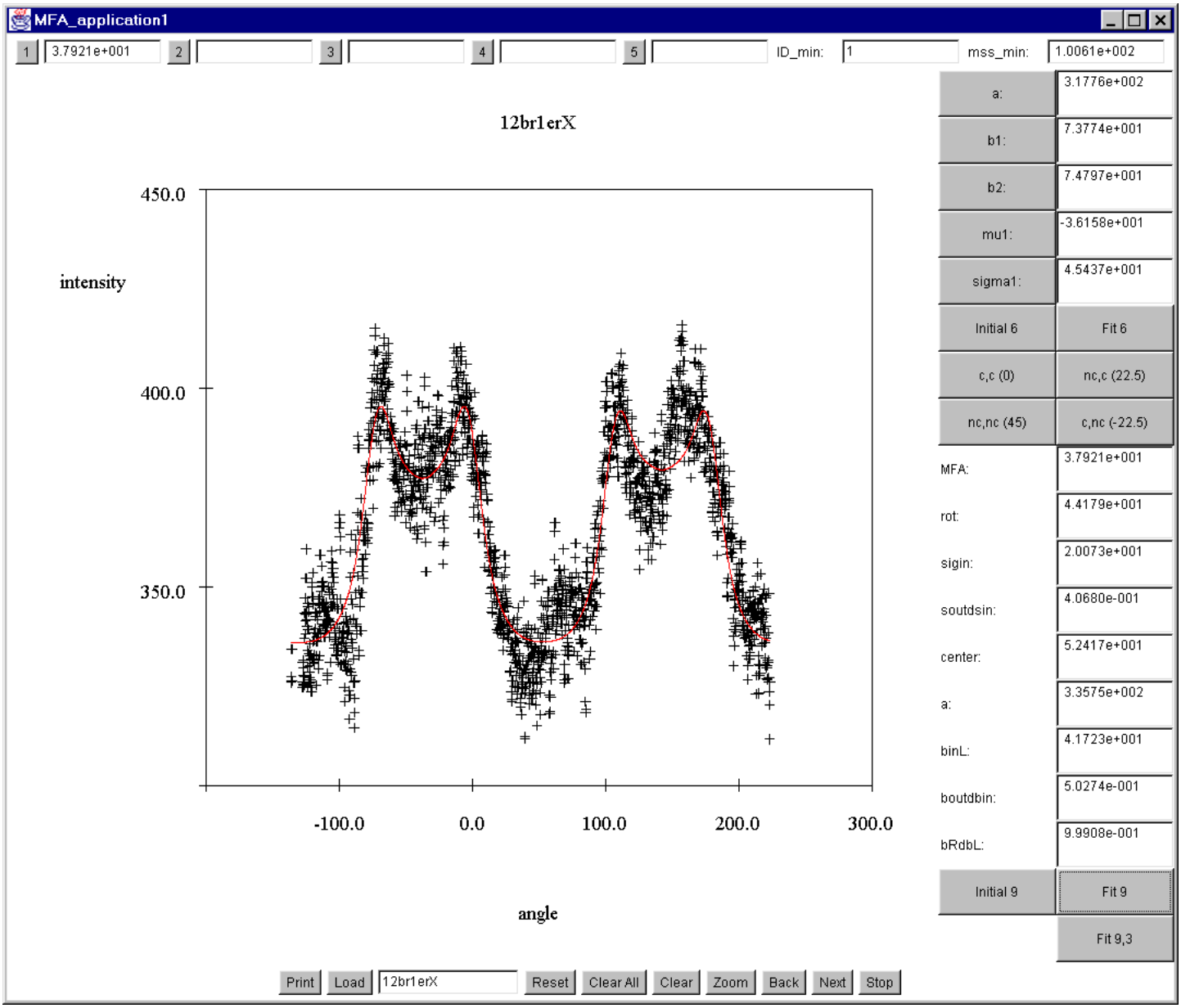

Figure 24: Main window for the application